ERDC TR-22-20

US Army Corps of Engineers®
Engineer Research and Development Center

ERDC
ENGINEER RESEARCH & DEVELOPMENT CENTER

Landform Identification in the Chihuahuan Desert for Dust Source Characterization Applications

Developing a Landform Reference Data Set

Samantha N. Cook, Matthew F. Bigl, Sandra L. LeGrand, Nicholas Webb, Gayle Tyree, and Ronald Treminio

September 2022

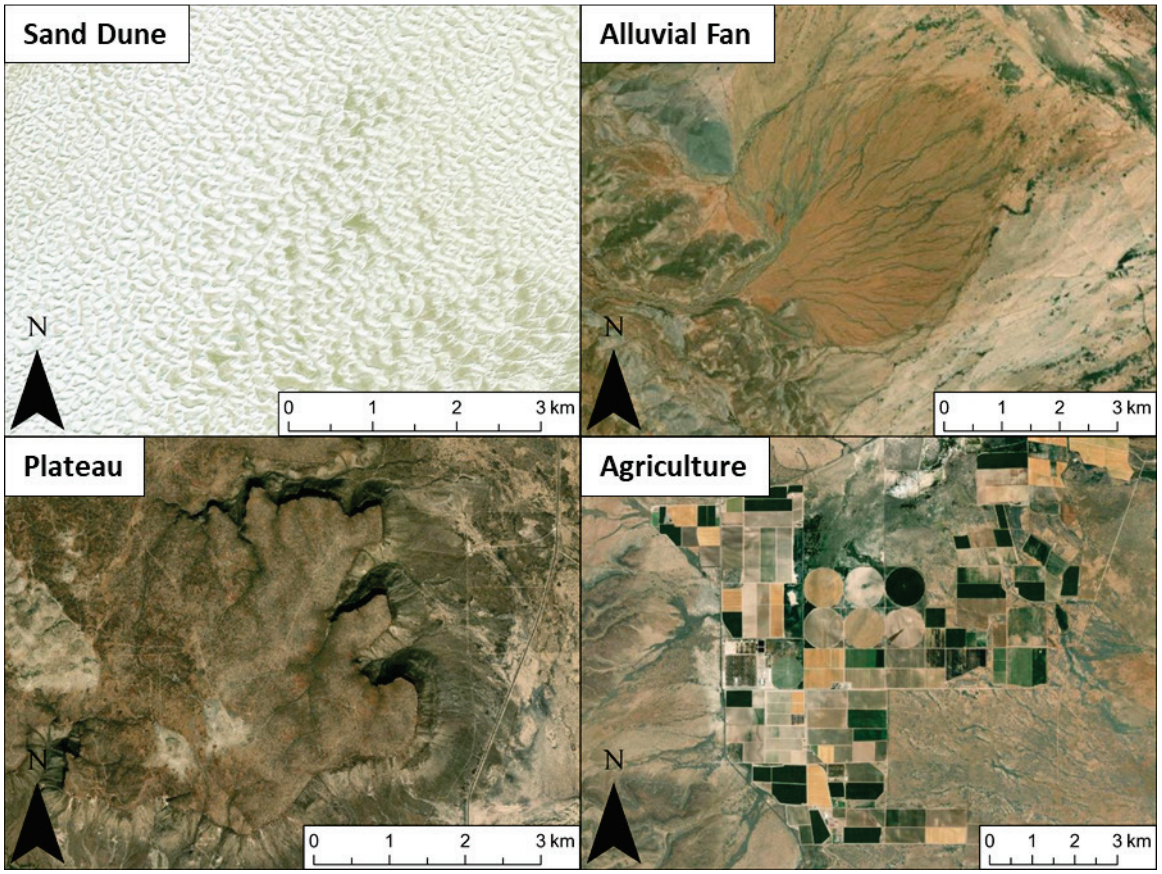

Engineer Research and Development Center

The US Army Engineer Research and Development Center (ERDC) solves the nation's toughest engineering and environmental challenges. ERDC develops innovative solutions in civil and military engineering, geospatial sciences, water resources, and environmental sciences for the Army, the Department of Defense, civilian agencies, and our nation's public good. Find out more at www.erdc.usace.army.mil.

To search for other technical reports published by ERDC, visit the ERDC online library at https://erdclibrary.on.worldcat.org/discovery.

ERDC TR-22-20
September 2022

Landform Identification in the Chihuahuan Desert for Dust Source Characterization Applications

Developing a Landform Reference Data Set

Samantha N. Cook and Matthew F. Bigl

US Army Engineer Research and Development Center (ERDC)
Cold Regions Research and Engineering Laboratory (CRREL)
72 Lyme Road
Hanover, NH 03755-1290

Sandra L. LeGrand

US Army Engineer Research and Development Center (ERDC)
Geospatial Research Laboratory (GRL)
7701 Telegraph Road
Alexandria, VA 22315-3864

Nicholas Webb, Gayle Tyree, and Ronald Treminio

USDA-ARS Jornada Experimental Range
MSC 3 JER, NMSU, Box 30003
Las Cruces, NM 88003

Technical Report (TR)

Prepared for Air Force Life Cycle Management Center
75 Vandenburg Drive, Building 1630
Hanscom Air Force Base, MA, 01731-2103

Under "Enhanced Dust Emission Characterization for Improved Atmospheric Dust Forecasting," MIPR F2BDAN1239G003

Abstract

ERDC-Geo is a surface erodibility parameterization developed to improve dust predictions in weather forecasting models. Geomorphic landform maps used in ERDC-Geo link surface dust emission potential to landform type. Using a previously generated southwest United States landform map as training data, a classification model based on machine learning (ML) was established to generate ERDC-Geo input data. To evaluate the ability of the ML model to accurately classify landforms, an independent reference landform data set was created for areas in the Chihuahuan Desert. The reference landform data set was generated using two separate mapping methodologies: one based on in situ observations, and another based on the interpretation of satellite imagery. Existing geospatial data layers and recommendations from local rangeland experts guided site selections for both in situ and remote landform identification. A total of 18 landform types were mapped across 128 sites in New Mexico, Texas, and Mexico using the in situ (31 sites) and remote (97 sites) techniques. The final data set is critical for evaluating the ML-classification model and, ultimately, for improving dust forecasting models.

Contents

Abstract ii

Figures and Tables v

Preface x

1 Introduction 1

1.1 Background 1
1.2 Objectives 2
1.3 Approach 2

2 Methodology 4

2.1 Study domain 4
2.2 Landform classes 5
2.3 Geospatial data sets 7
2.4 Data processing and analysis 8
2.5 Field methodology 9
2.6 Remote landform identification 9

3 Results 11

3.1 In situ mapping results 11
3.2 Remote mapping results 17
3.3 Individual landform type results 22
3.3.1 Sand dune 22
3.3.2 Interdune 24
3.3.3 Sand sheet 25
3.3.4 Sand plain 26
3.3.5 Alluvial fan 27
3.3.6 Alluvial plain 29
3.3.7 Fluvial terrace 30
3.3.8 Playa 33
3.3.9 Plateau 34
3.3.10 Recent volcanic feature 35
3.3.11 Pediment 36
3.3.12 Badlands 38
3.3.13 Wind erosional feature 38
3.3.14 Agriculture 39
3.3.15 Bedrock 40
3.3.16 Fine-grained lake deposit 41
3.3.17 Urban 42
3.3.18 Water 43
3.4 Independent reference landform data set 45

4 Conclusions and Recommendations 50

References 53

Appendix: Landform Types in This Study 57

Abbreviations 67

Report Documentation Page 68

Figures and Tables

Figures

1. General overview of the fieldwork areas in the Chihuahuan Desert in Mexico, New Mexico, and Texas. Arizona and the border between the United States and Mexico are also shown. The Chihuahuan Desert is depicted by the *light pink polygon*. The inset map (*top right*) shows the location of the field area relative to North America. 4
2. Overview of the in situ and remote landform locations in New Mexico, Texas, and Mexico. The locations of the 31 in situ landform sites in New Mexico are shown by the *red circles*, while the 97 landform sites assessed via satellite imagery interpretation in Mexico, New Mexico, and Texas are shown by the *yellow circles*. 11
3. Overview of all in situ field sampling locations in southern New Mexico; 11 landform types were identified at 31 field sites. The 31 landform sites are shown as *color-categorized circles*. 12
4. Overview of all remotely identified landform locations in Mexico, New Mexico, and Texas; 15 landform types were identified at 97 field sites. The 97 landform sites are shown as *color-categorized circles*. 17
5. Overview photo of a gypsum sand dune observed by the field team. 23
6. *Top*: Satellite image of a remotely mapped sand dune location. The *yellow circle* represents the actual field site for this landform. *Bottom*: Satellite image of a dune field that depicts the regular, repeating, undulating structure typical of this landform type. 24
7. Overview photo of a gypsum interdune observed by the field team. 25
8. Overview photo of a sand sheet observed by the field team. 25
9. Satellite image of a remotely mapped sand sheet location. The *yellow circle* represents the actual field site for this landform. 26
10. Overview photo of a sand plain observed by the field team. 27
11. Overview photo of an alluvial fan observed by the field team. 27
12. Satellite images of two remotely mapped alluvial fans. The *yellow circles* represent the actual field site for each landform. *Bottom*: This remotely mapped alluvial fan does not display typical fan morphology, which may be caused by interference from the outcropping rocky knob (outlined by the *red rectangle*) located directly west of the yellow point. 28
13. Overview photo of an alluvial plain observed by the field team. 29
14. Satellite image of a remotely mapped alluvial plain location. The *yellow circle* represents the actual field site for this landform. 30
15. *Top*: Overview photo of a fluvial terrace observed by the field team. *Bottom*: Sedimentological changes noted on this fluvial terrace, which varied from light-colored chalky sediment to light-brown sand. 31
16. Satellite image of two remotely mapped fluvial terraces. The *yellow circles* represent the actual field sites for each landform, though the *yellow marker* in the bottom panel is estimated to be located approximately 50 m east of the true landform location. 32

17. Overview photo of a playa observed by the field team. 33
18. Satellite image of a remotely mapped playa field site. The *yellow circle* represents the actual location of this landform. 34
19. Overview photo of a plateau observed by the field team. 34
20. Satellite image of a remotely mapped plateau field site. The *yellow circle* represents the actual location of this landform. 35
21. Overview photo of a recent volcanic feature observed by the field team. 36
22. Overview photo of a pediment field site that was observed by the field team and was interpreted and reclassified as an alluvial plain. 36
23. Satellite images of remotely mapped pediment field sites. The *yellow circles* represent the actual locations of each landform. *Bottom*: Pediment labeled with a medium level of confidence. The lobate or leaf shape of this landform suggests it could be an alluvial fan. Because a distinction between an alluvial fan and a pediment could not be made at this site, the confidence level was reduced to medium 37
24. Satellite image of a remotely identified badlands field site that was later determined to be misclassified. The *yellow circle* that represents the actual location for this landform was reclassified as a bedrock cliff by the field team. To see satellite imagery of an actual badlands site, see the Appendix. 38
25. Satellite image of a remotely mapped wind erosional feature. The *yellow circle* represents the actual location of this wind erosional feature. 39
26. Satellite image of a remotely mapped agricultural feature. The *yellow circle* represents the actual location of this agricultural feature. 40
27. Satellite image of a remotely mapped bedrock feature. The *yellow circle* represents the actual location of this bedrock feature. 41
28. Satellite image of a remotely mapped fine-grained lake deposit that was confirmed by a secondary source. The *yellow circle* represents the actual location of the fine-grained lake deposit. 42
29. Satellite image of a remotely mapped urban location. The *yellow circle* represents the relative center of the site. 43
30. Satellite image of a remotely mapped water feature. The *yellow circle* represents the actual location of this water feature. 44
31. Water features at different map scales showing changes in feature dimensions, or lack thereof, through time. The two *upper* panels depict the same general region at two different resolutions. At a coarser map scale (*top left*), a water feature is depicted, while at a finer map scale (*top right*), a salt flat is depicted. Conversely, the two *bottom* panels depict a water feature that has roughly the same dimensions at both coarse and fine map resolutions, which suggests it is a permanent water feature. 44
32. *Top*: Stabilized sand dune, also shown in Fig. 6, that highlights the difficulty in deciphering between sand dunes, interdunes, and wind erosional features. *Bottom*: Pediment, also shown in Fig. 23, that displays the difficulty in differentiating pediments from fans, particularly without elevation data to support classification labels. 51
A-1. Alluvial fans are “moderately- to gently-sloping constructional landforms that are composed of unconsolidated clastic sediment primarily derived from eroding highlands. The clastic materials typically consist of abundant gravel (>2 mm in

diameter) and sand with lesser amounts of silt and clay. Alluvial fans typically occur on the upper margins of piedmont slopes that flank mountain highlands, plateaus, pediments, and badlands." (McDonald, Adams, et al. 2020, 13). The approximate extent of the landform is shown by the *red dashed line*. 57

A-2. Alluvial plains are "low-gradient landforms found along basin floors that are generally the floodplains of major axial streams. Deposits typically consist mostly of stratified, well- to moderately-sorted sand with lesser silt/clay and gravel. Sand sheets and sand sea/dunes often accumulate within alluvial plains downwind of playas. Vegetation cover is often found within the margins of alluvial plains along the banks of perennial or ephemeral streams or as isolated areas at alluvial fan and plain contacts associated with spring discharge" (McDonald, Adams, et al. 2020, 13). The approximate extent of the landform is shown by the area between the *red dashed lines*. 58

A-3. A dune field showing sand dunes (white, wind-blown sand) and interdunes (tan sandy features separating the sand dunes). Sand dunes are "areas consisting of mounds, ridges, or hills of wind-blown sand, either bare or covered with vegetation, that are composed of loose and well-sorted sand and minor silt. Extensive areas of covered sand are referred to as sandy plains, dune fields or sand sea (also called ergs). These features occur where sand-rich sediment supply is plentiful" (McDonald, Adams, et al. 2020, 15). An interdune is "the relatively flat surface, whether sand-free or sand-covered, between dunes" (Schoeneberger and Wysocki 2017, 629-39). 58

A-4. Pediments are "erosional slopes or erosion surfaces that lie at the foot of mountain highlands or plateaus, which typically exhibit a concave upward profile. Pediment surfaces are typically broad and gently-sloping (2°–19°), cut into bedrock, commonly marginal to mountain highlands. Pediments may be bare or mantled with a thin layer of surficial sediment or rocks on the surface that form desert pavements" (McDonald, Adams, et al. 2020, 14). The approximate extent of the landform is shown by the area between the *red dashed lines*. 59

A-5. A plateau is "a relatively elevated area of comparatively flat land composed of well-indurated bedrock, which is commonly limited on at least one side by an abrupt descent to lower ground. Plateaus form extensive areas of land that rise 150–300 m above the adjacent country or above sea level and commonly fringe mountain highlands. It is higher than a plain and more extensive than a mesa. Plateaus are commonly covered by a thin cap of silt-rich soil (loess)" (McDonald, Adams, et al. 2020, 14). The most distal edge of several plateaus is approximated by the *red dashed line*. 59

A-6. A playa is "an ephemerally flooded, barren area on a basin floor that is characterized by fine-grained sedimentary deposition by floods in recent times and/or during previous pluvial episodes. Playas are typically located at the depocenter within a basin or lowland area" (McDonald, Adams, et al. 2020, 14). The approximate extent of the landform is shown by the *red dashed line*. 60

A-7. Recent volcanic features are "landforms that have been recently formed from volcanic activity. The common type of recent volcanics is basalt flows and fields (plateaus) and volcanic vents (i.e., cinder cones, shield volcanos, lava flows, etc.)" (McDonald, Adams, et al. 2020, 15). The approximate extent of the landform is shown by the *red dashed line*. 60

A-8. A sand plain is "a sand-covered plain, which may originate by deflation of sand dunes, and whose lower limit of erosion is governed by the water table"

(Schoeneberger and Wysocki 2017, 629-62). The approximate extent of the landform is shown by the *red dashed line*. 61

A-9. Sand sheets are "sedimentary plains covered in fine sediments composed of loose and well-sorted sand to packed silt or clay. In systems of large linear dunes, these may include the troughs between dunes or may be associated with climbing dunes on alluvial fan surfaces" (McDonald, Adams, et al. 2020, 15). The approximate extent of the landform is contained within the *red dashed polygon*. 61

A-10. Fluvial terraces are "stream or river terraces located adjacent to, but above, stream or river channels and flood plains" (McDonald, Adams, et al. 2020, 13). The approximate extent of the landform is shown by the area between the red dashed lines. 62

A-11. Wind erosional features are "erosional features that typically exhibit an elongate ridge or series of ridges carved by wind erosion. The ridges are parallel to the prevailing wind direction and predominantly form on poorly- to moderately-consolidated sediment" (McDonald, Adams, et al. 2020, 15). The approximate extent of the landform is shown by the area within the rectangle delineated by the *red dashed line*. 62

A-12. Badlands: is "a landform that exhibits a complex stream-dissected topography consisting of deep, narrow ephemeral washes alternating with abundant, sharp and narrow ridge tops. Surfaces commonly have little or no vegetative cover, are highly erosive, and with no or minimal development of soils. Underlying material is generally unconsolidated or weakly indurated sediment largely composed of mixtures of clay, silt, and sand. Soluble salts of gypsum and halite are common" (McDonald, Adams, et al. 2020, 14). Badlands are highly expansive, and most of the image, excluding the river channels, displays badlands. 63

A-13. Agriculture is defined as "a human-modified 'landscape' dominated by permanent, extensive alterations to the physical shape and/or internal stratigraphy of the land due to agricultural management for food, fiber or forage production, that have substantively altered water flow and sediment transport across and within the regolith (e.g., leveled land). Commonly excludes areas of minor alterations (e.g., shallow plowing) that are easily obscured or obliterated by natural bio-, pedo-, or cryoturbation" (Schoeneberger and Wysocki 2017, 629-4). The approximate extent of the agriculture area is shown by the *red dashed polygon*. 64

A-14. Bedrock is "a general term for the solid rock that underlies the soil and other unconsolidated material or that is exposed at the surface" (Schoeneberger and Wysocki 2017, 629-10). The approximate extent of the bedrock area is shown by the *red dashed polygon*. 65

A-15. Fine-grained lake deposits "are typically light colored, fine-grained (e.g., high silt and clay content) lake deposits found in basin bottoms and rimming playas. May or may not be eroded into badland forms" (McDonald, Adams, et al. 2020, 14). The approximate extent of the fine-grained lake deposit is shown by the *red dashed polygon*. 65

A-16. Urban areas are "areas of extensive urban/suburban/industrial development where soil surface is modified and covered by buildings and infrastructure" (McDonald, Adams, et al. 2020, 16). The approximate extent of the urban area is shown by the *red dashed polygon*. 66

A-17. Water refers to "open bodies of water including reservoirs, lakes, seas, and

rivers" (McDonald, Adams, et al. 2020, 16). The approximate extent of the water feature is shown by the *red dashed polygon*. 66

Tables

1. Comparison of the landform reference classification scheme used in this study and the McDonald, Adams, et al. (2020) SWUS landform map classification scheme. Landforms with subgroups (e.g., alluvial fans, alluvial plains, and fluvial terraces) and the playa, plateau, and bedrock categories were combined into single classes. Landforms that were not present in the fieldwork area were not included in this classification scheme. 6

2. Group 1: sand feature landform data. Asterisks denote landform classifications deemed incorrect by the field team. The field team's suggested landform type is listed in parentheses beneath each incorrect classification. Latitude and longitude are reported in decimal degrees (DD). 13

3. Group 2: fluvial feature landform data. Asterisks denote landform classifications deemed incorrect by the field team. The field team's suggested landform type is listed in parentheses beneath each incorrect classification. 14

4. Group 3: all other features landform data. Asterisks denote landform classifications deemed incorrect by the field team. The field team's suggested landform type is listed in parentheses beneath each incorrect classification. 16

5. All landforms identified through remote satellite interpretation. The confidence level associated with each landform site expresses the mapper's confidence in each classification. A high level of confidence was assigned to features with a classic geomorphic expression, meaning the landforms had easily identifiable characteristics. Sand sheets and sand plains could not be differentiated from one another using satellite imagery alone, but they could be classified as either/or with a high degree of certainty. Therefore, the high level of confidence assigned to the sand sheets and sand plains, as noted with an asterisk, represents confidence that the landform is one of those two landform types. 18

6. Final independent reference landform data set mapped in this study. All landforms mapped remotely and in person are listed and compared to their respective McDonald, Adams, et al. (2020) SWUS landform map classification. The four landforms the field team deemed incorrectly classified are marked with an asterisk, and the alternative landform-type designation suggested by the field team is listed. The two alluvial plain sites with asterisks were originally misclassified as a fluvial terrace and a pediment, while the two bedrock sites with asterisks were originally misclassified as badlands and a fluvial terrace. 45

Preface

This study was sponsored by the Air Force Life Cycle Management Center (AFLCMC) under project "Enhanced Dust Emission Characterization for Improved Atmospheric Dust Forecasting." Funding was provided by MIPR F2BDAN1239G003.

The work was performed by the Terrestrial and Cryospheric Sciences Branch (Dr. John W. Weatherly, chief) and the Engineering Resources Branch (Dr. Melisa Nallar, acting chief) of the Research and Engineering Division, US Army Engineer Research and Development Center, Cold Regions Research and Engineering Laboratory (ERDC-CRREL). At the time of publication, Dr. Caitlin A. Callaghan was division chief. The acting deputy director of ERDC-CRREL was Mr. Bryan E. Baker, and the director was Dr. Joseph L. Corriveau.

Additional work was performed by the Information Generation and Management Branch (Mr. Michael F. Mailloux, chief) of the Geospatial Research Division, ERDC Geospatial Research Laboratory (GRL). At the time of publication, Mr. Jeffrey B. Murphy was division chief. The acting director of ERDC-GRL was Ms. Valerie L. Carney.

Researchers from ERDC collaborated with New Mexico State University's College of Agricultural, Consumer, and Environmental Sciences of Las Cruces, New Mexico. Dr. Dorothea Lundberg and Mr. Taylor Hodgdon, ERDC-CRREL, provided manuscript technical review comments, and Dr. Travis Nauman provided subject matter expertise in early review stages of this report.

The commander of ERDC was COL Christian Patterson, and the director was Dr. David W. Pittman.

1 Introduction

1.1 Background

Airborne dust particles can create adverse air quality conditions, abrasion hazards for personnel and equipment, and degraded visibility (De Longueville et al. 2010; Okin et al. 2011; Sprigg et al. 2014; Middleton 2017; Schweitzer et al. 2018; Bhattachan et al. 2019; Rushingabigwi et al. 2020). Accordingly, accurate characterizations of terrain dust emission potentials are critical for mission planning and land management decisions, especially in dryland environments (Department of the Army 2019). However, the processes that control the spatial heterogeneity of surface dust source strength are not fully understood (Richter and Gill 2018). Several previous studies argue that a location's dust emission potential reflects its geomorphology (i.e., the physical, chemical, and biological processes that shape the landscape into distinct landform types; Wang et al. 2006; Bullard et al. 2008; Wang et al. 2008; Sweeney et al. 2011; Baddock et al. 2016; Parajuli and Zender 2017). Therefore, geomorphic landform designations can serve as an analog for dust emission potential because landscape formation processes also affect soil-state evolution (Bullard et al. 2011; Parajuli et al. 2014; Bacon and McDonald 2016; McDonald, Adams, et al. 2020; McDonald, Hartshorn, et al. 2020).

Researchers from the Desert Research Institute (DRI) established a series of landform classes common to most desert environments (Bacon, McDonald, Amit, et al. 2011; Bacon and McDonald 2016; McDonald, Adams, et al. 2020). After establishing the landform classification scheme, analysts from DRI and the University of South Dakota assigned characteristic dust emission potential values to each landform class based on in situ measurements (Sweeney et al. 2011; McDonald, Hartshorn, et al. 2020). These methods enabled the generation of regional-scale dust emission potential data sets, with landforms mapped through subjective satellite and aerial imagery interpretation (Bacon, McDonald, Amit, et al. 2011; Bacon, McDonald, and Green 2011; Sweeney et al. 2011; McDonald, Hartshorn, et al. 2020). Regional dust emission potential maps created using this technique have since been used to support dust hazard identification and dust event forecasting (e.g., McDonald, Adams, et al. 2020; LeGrand and Brooks 2018). However, the map generation process required costly and

time-consuming manual landform classification by expert geomorphologists.

1.2 Objectives

At present, there are two landform maps available for the analog approach to dust emission potential characterization, including a 1:750,000 scale map of Southwest Asia (Bacon and McDonald 2016) and a 1:100,000 scale map of portions of the Mojave and Sonoran Deserts in the southwest United States (SWUS; McDonald, Adams, et al. 2020). Recently, ERDC researchers have begun exploring machine learning (ML) techniques to expand the spatial coverage of these existing maps to global coverage for nonpolar desert regions (Hodgdon et al. 2021). To develop a model, analysts will require validation data from new domains to determine if the resultant modeling capabilities are portable to regions outside of the original model training areas in Southwest Asia and the SWUS. The purpose of this effort was to establish an independent landform reference data set to support these validation efforts using sites from the Chihuahuan Desert in the SWUS. The ecology, landform distribution, and mineralogy of this desert are markedly different from those of the previously mapped locations. However, this effort was not meant to be a census of landforms in the region but, instead, an accurate collection of an independent landform data set to be used for model validation.

1.3 Approach

For this effort, we created a landform classification scheme adapted from the McDonald, Adams, et al. (2020) SWUS landform map (Section 2.2). Specifically, we established two landform mapping methodologies to acquire examples of landform sites from the adapted classification scheme: one based on in situ observations, and another based on the interpretation of satellite imagery. In both methods, existing geospatial data layers guided our initial site selections and landform-type assumptions. For the in situ inspections, analysts followed a series of standardized field procedures to interpret key terrain attributes associated with each site. For the satellite-based methodology, analysts assessed landform locations by examining Esri et al.'s (2021) Geographic Information System (GIS) World Imagery basemap. We only mapped landforms via the imagery-interpretation method if a clear distinction of landform type was possible from satellite imagery interpretation alone or if supporting literature confirmed the

suspected landform classification. We then supplemented the site consideration list with recommendations from local rangeland subject matter experts (SMEs), who identified additional potential field sites by analyzing the same GIS basemap imagery.

Section 2 of this report details the methodologies, lists the landform classifications, and describes the geospatial data sets used in this effort. Section 3 highlights the results from both the in situ field observations and the satellite interpretations. Last, Section 4 discusses the conclusions of this research.

2 Methodology

For this study, we considered geomorphic landforms for mapping in a subregion of the Chihuahuan Desert in northern Mexico, southern New Mexico, and western Texas (Figure 1). All of the field sites we assessed in person were in New Mexico, while the locations examined via satellite imagery were in Mexico, New Mexico, and Texas. For both methods, we conducted a geospatial analysis using ArcGIS Pro 2.8 to review preexisting landform and soil data sets from the USDA (n.d.a), the Bureau of Land Management (BLM; n.d.), the Natural Resources and Conservation Service (NRCS; USDA n.d.c), satellite imagery, and the knowledge of the local geomorphology SMEs. Geospatial data sets of landform types (using different classification schema), soil morphology, land use, zoning, and road networks supported landform identification and planning for in situ landform confirmation and measurements.

Figure 1. General overview of the fieldwork areas in the Chihuahuan Desert in Mexico, New Mexico, and Texas. Arizona and the border between the United States and Mexico are also shown. The Chihuahuan Desert is depicted by the *light pink polygon*. The inset map (*top right*) shows the location of the field area relative to North America.

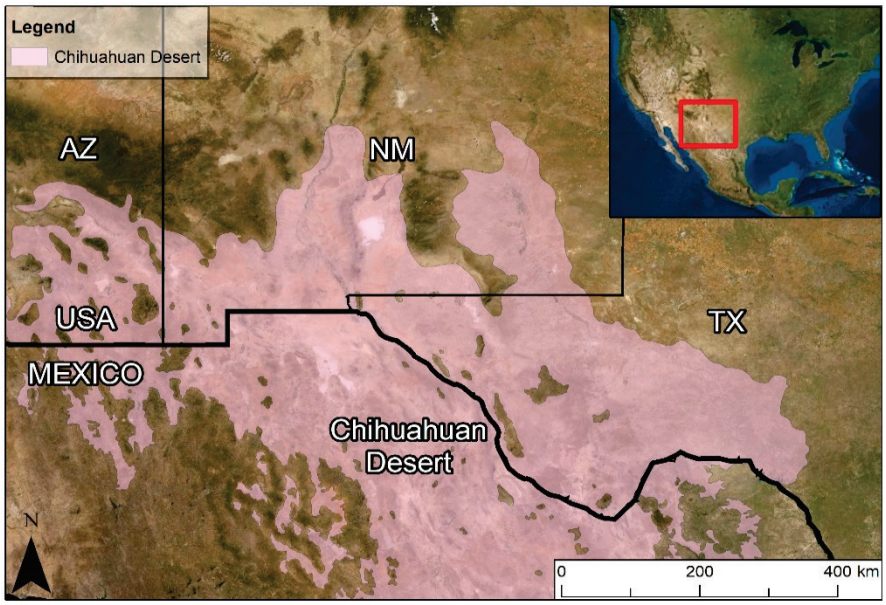

2.1 Study domain

The Chihuahuan Desert is the largest desert in North America, covering over 250,000 square miles and spanning two countries (i.e., the United

States and Mexico), and is the most biologically diverse desert in the western hemisphere (NPS n.d.). The area receives most of its rainfall during the summer monsoon season (approximately July through September) and tends to get more summer rainfall than other desert environments in the United States (NPS n.d.). In addition, the landscape of the Chihuahuan Desert is higher in elevation than the neighboring Sonoran Desert (Scarborough 2000; Sleeter et al. 2012). The landforms commonly found within the Chihuahuan Desert include broad basins flanked by alluvial fans, fluvial terraces, and broad, flat-topped features such as plateaus and mesas. In the adjacent Sonoran Desert, typical landforms include alluvial fans, pediments, fluvial terraces, and floodplains (Scarborough 2000; Sleeter et al. 2012).

2.2 Landform classes

For this study, we chose to use a variation of McDonald, Adams, et al.'s (2020) 32-class scheme for our reference data collection to support verification activities. The 32-class scheme stems from the 17 original landform classes set by Bacon, McDonald, and Green (2011) and Bacon and McDonald (2016), but it also includes additional age- or wetness-based subclassifications, more fluvial landform types, and categories for urban (i.e., developed) areas and agriculture.

Not all landform types incorporated into the McDonald, Adams, et al. (2020) SWUS landform map were present in the study area. Furthermore, some classes in the SWUS landform map scheme, such as the age-based landform categories (e.g., old versus young alluvial fans), are challenging to discern without using disruptive field methods (e.g., digging soil pits). To avoid trespassing or causing project delays by engaging in activities that required permitting, we limited our field assessment methodology to nondestructive observation techniques that we could accomplish from public access areas. This meant that where age-based subclassifications would have been appropriate, a broader landform type was used to capture both young and old features. For this study, we examined sand dunes, interdunes, sand sheets, sand plains, alluvial fans, alluvial plains, fluvial terraces, playas, plateaus, recent volcanic features, pediments, wind erosional features, badlands, bedrock, agriculture, water, urban, and fine-grained lake deposits (see the Appendix for detailed descriptions of each landform type). These landform classes also aligned with the scheme used by the BLM (Herrick et al. 2017) and the USDA (n.d.c), which differs slightly from the scheme used for the McDonald, Adams, et al. (2020) SWUS data

set. We chose to follow the BLM and USDA classes for our initial analysis because most geospatial data layers available for the Chihuahuan Desert region adopted the BLM's and USDA's landform-type labels. Table 1 shows how the BLM and USDA landform categories (referred to henceforth as the *reference classification scheme*) compare to the McDonald, Adams, et al. (2020) SWUS landform map classes.

The reference classification scheme used herein also includes two landform types that McDonald, Adams, et al. (2020) did not incorporate: interdunes and sand plains. The McDonald, Adams, et al. scheme treats these landform types as part of the sand dune and sand sheet classes, respectively. Even though the interdune–sand dune and sand plain–sand sheet pairings are similar in terms of their dust emission potential and geomorphology, we maintained these as separate classes in the reference classification scheme to offer additional insight during future model validation efforts.

Table 1. Comparison of the landform reference classification scheme used in this study and the McDonald, Adams, et al. (2020) SWUS landform map classification scheme. Landforms with subgroups (e.g., alluvial fans, alluvial plains, and fluvial terraces) and the playa, plateau, and bedrock categories were combined into single classes. Landforms that were not present in the fieldwork area were not included in this classification scheme.

Reference Classification Scheme	McDonald, Adams, et al. (2020) SWUS Landform Map Classification Scheme	Comments
Sand dune	Sand dune	
Interdune	Sand dune	Present in field and comparable to sand dunes
Sand sheet	Sand sheet	
Sand plain	Sand sheet	Present in field and comparable to sand sheets
Alluvial fan	Alluvial fan (young, intermediate, old); alluvial fan and sand sheet	
Alluvial plain	Alluvial plain (young and old)	
Fluvial terrace	Fluvial terrace (young and old)	
Playa	Wet and dry playa	
Plateau	Plateau; plateau and sand sheet	
Recent volcanic feature	Recent volcanic feature	

Table 1 (cont.). Comparison of the landform reference classification scheme used in this study and the McDonald, Adams, et al. (2020) SWUS landform map classification scheme. Landforms with subgroups (e.g., alluvial fans, alluvial plains, and fluvial terraces) and the playa, plateau, and bedrock categories were combined into single classes. Landforms that were not present in the fieldwork area were not included in this classification scheme.

Reference Classification Scheme	McDonald, Adams, et al. (2020) SWUS Landform Map Classification Scheme	Comments
Pediment	Pediment	
Wind erosional feature	Wind erosional feature	Observed only though satellite imagery
Badlands	Badlands	Observed only through satellite imagery
Bedrock	Bedrock; sand on bedrock	Observed only through satellite imagery
Agriculture	Agriculture	Observed only through satellite imagery
Water	Water	Observed only through satellite imagery
Urban	Urban or developed areas	Observed only through satellite imagery
Fine-grained lake deposit	Fine-grained lake deposit	Observed only through satellite imagery
N/A	Active wash	Not identified in field area
N/A	Open mine/tailings	Not identified in field area
N/A	Landslide feature	Not identified in field area
N/A	Undifferentiated surficial deposit	Not identified in field area
N/A	Broad river valley	Not identified in field area
N/A	Coastal feature	Not identified in field area
N/A	Delta plain	Not identified in field area
N/A	Pluvial lake	Not identified in field area

2.3 Geospatial data sets

BLM's (n.d.) Assessment, Inventory, and Monitoring (AIM) data set and the USDA's (n.d.c) NRCS data set were the primary landform data sets used for field planning. The AIM data set is a point shapefile containing information related to terrestrial ecosystems, such as plant, soil, and landform classifications, across the western United States (BLM n.d.). The

NRCS data set includes landform classification point data from the National Soil Information System (NASIS; USDA n.d.b), which consists of points across the United States from the NRCS pedon database, and a soil map product from the Soil Survey Geographic database (SSURGO; Shawn Salley, email message to author, 17 February 2021; USDA n.d.a).

To refine potential in situ landform mapping locations and develop routes between field sites, we examined GIS layers of the Chihuahuan Desert boundary, the United States roadway system, and public land in New Mexico. To determine land accessibility, we also reviewed the Protected Areas Database of the United States (PAD-US) version 2.1 (USGS 2020). The PAD-US data were in the form of an ArcGIS web service layer originating from the USGS and contained information related to protected areas, including public land and private protected areas, and the level of access to these lands. The different categories of land access in the PAD-US data included open, restricted (e.g., permit or seasonal), closed, and unknown. For this effort, we only visited public access lands and avoided privatively owned locations.

2.4 Data processing and analysis

We clipped the NRCS (USDA n.d.c) and AIM (BLM n.d.) point data for our fieldwork area of interest, using boundary layers of the Chihuahuan Desert and New Mexico as our domain limits. Next, we refined the data by exporting only the points for the landform types of interest listed in Table 1. Although there were approximately 51,000 points in the NRCS and AIM data at the beginning of this analysis, few points had specific landform classifications listed, some had only soil texture information, and others were too broad to fit into any of the landform classifications used in this study. Therefore, the number of useful points lessened substantially during these data processing steps, and only those locations described in Sections 3.1 and 3.2 were included in this study. Using roadway layers for New Mexico, we further narrowed groups of points for in situ confirmation so that field crews could easily navigate to and from each site and sample all necessary landforms within a multiday fieldwork campaign. Once we had selected our initial point locations, local rangeland and geomorphology SMEs reviewed our potential sampling areas. Points that SMEs were not able to visit were saved as potential sites to be used in the remotely sensed data set.

2.5 Field methodology

All field analysts followed a standardized methodology to ensure procedures were consistent at each site. Site names incorporated an MM-DD-Site number labeling scheme, where *MM* and *DD* represent the month and day of the fieldwork, respectively. To help organize the site photographs, the first photograph taken at each site was of a whiteboard with the site name written on it. Analysts noted the date, time, and approximate weather conditions (i.e., percent cloud coverage, temperature, and general conditions) and recorded their subjective evaluations of the site to verify the initial landform classifications provided by the geospatial data set. If the analysts perceived a classification to be incorrect, they provided reasons for their conclusion and suggested an alternate landform-type designation. Field analysts also recorded landform attributes, including percent coverage by vegetation, surface soil characteristics, and level of disturbance, along with any unusual or unique aspects of the site. The soil characteristics that were noted were based on the SME's visual estimation because digging was not permitted at all sites, and therefore, traditional soil pit analyses could not be conducted. In addition, the analysts recorded a GPS waypoint in decimal degrees using a handheld Garmin GPSMAP 62sc GPS unit and the World Geodetic System 1984 (WGS84) datum and noted the approximate location of the waypoint relative to the overall landform (e.g., center of the landform or northern edge of the landform). Finally, the field analysts took photographs from the waypoint in each cardinal direction and at least one picture characterizing the surface soil and sedimentology of the site

2.6 Remote landform identification

We expanded on the in situ reference data set collections by reviewing and interpreting satellite imagery acquired through the ArcGIS Pro basemap function (Esri et al. 2021). Across the field-study area in the Chihuahuan Desert, this imagery consisted of WorldView-2, -3, and -4 and GeoEye-1 imagery, with collection years ranging from 2017 to 2020 (Esri et al. 2021). The actual image collection dates varied based on location because this is a large mosaic of imagery collected over a multiyear timeframe. Satellite imagery was reviewed primarily at 1:50,000 and 1:100,000 to identify landforms. For all landforms identified via the imagery-interpretation technique, mappers assigned a high, medium, or low confidence level to single points selected to represent the location of a given landform. This

confidence level, or quality score, reflects the analyst's confidence in landform selection and is highly subjective. Analysts only indicated a "high" confidence level when they were certain of the classification of the given landform. A "medium" confidence level was assigned when the analyst was almost certain, but not entirely confident, of the landform classification, and a "low" confidence level was assigned when the analyst had the lowest level of confidence in the landform classification. Incorporating this remote-mapping methodology enabled us to include additional landform types and sites in Mexico, New Mexico, and Texas that we would have otherwise had to exclude due to accessibility issues or travel constraints. By creating point features for easily identifiable landforms, such as urban areas, agriculture, water, bedrock, and so on, the overall number of validation points was increased substantially while ensuring the accuracy of the identifications.

3 Results

We identified a total of 128 landform sites located in New Mexico, Texas, and Mexico using both in situ (31 sites) and remote mapping (97 sites) techniques (Figure 2). These sites included 18 different landform types, including 3 sand dunes, 2 interdunes, 7 sand sheets, 1 sand plain, 13 alluvial fans, 8 alluvial plains, 7 fluvial terraces, 15 playas, 14 plateaus, 2 recent volcanic features, 3 pediments, 1 badlands, 13 agriculture, 11 bedrock, 8 fine-grained lake deposits, 10 urban, 9 water, and 1 wind erosional feature, mapped via in situ and remote techniques.

Figure 2. Overview of the in situ and remote landform locations in New Mexico, Texas, and Mexico. The locations of the 31 in situ landform sites in New Mexico are shown by the *red circles*, while the 97 landform sites assessed via satellite imagery interpretation in Mexico, New Mexico, and Texas are shown by the *yellow circles*.

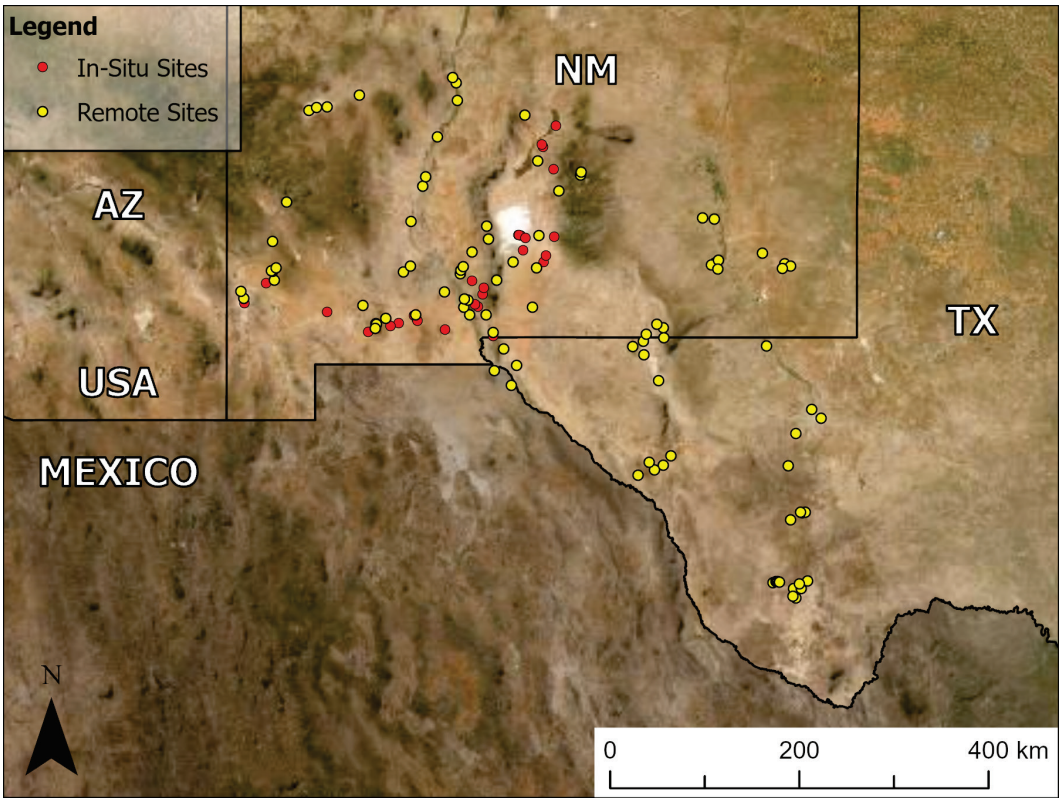

3.1 In situ mapping results

Field crews assessed 31 individual landform sites located in the southern region of New Mexico. Figure 3 shows the 11 different landform types, including 2 sand dunes, 2 interdunes, 3 sand sheets, 1 sand plain, 4 alluvial

fans, 6 alluvial plains, 3 fluvial terraces, 6 playas, 1 plateau, 2 recent volcanic features, and 1 pediment, that were represented at the 31 field sites.

Figure 3. Overview of all in situ field sampling locations in southern New Mexico; 11 landform types were identified at 31 field sites. The 31 landform sites are shown as *color-categorized circles*.

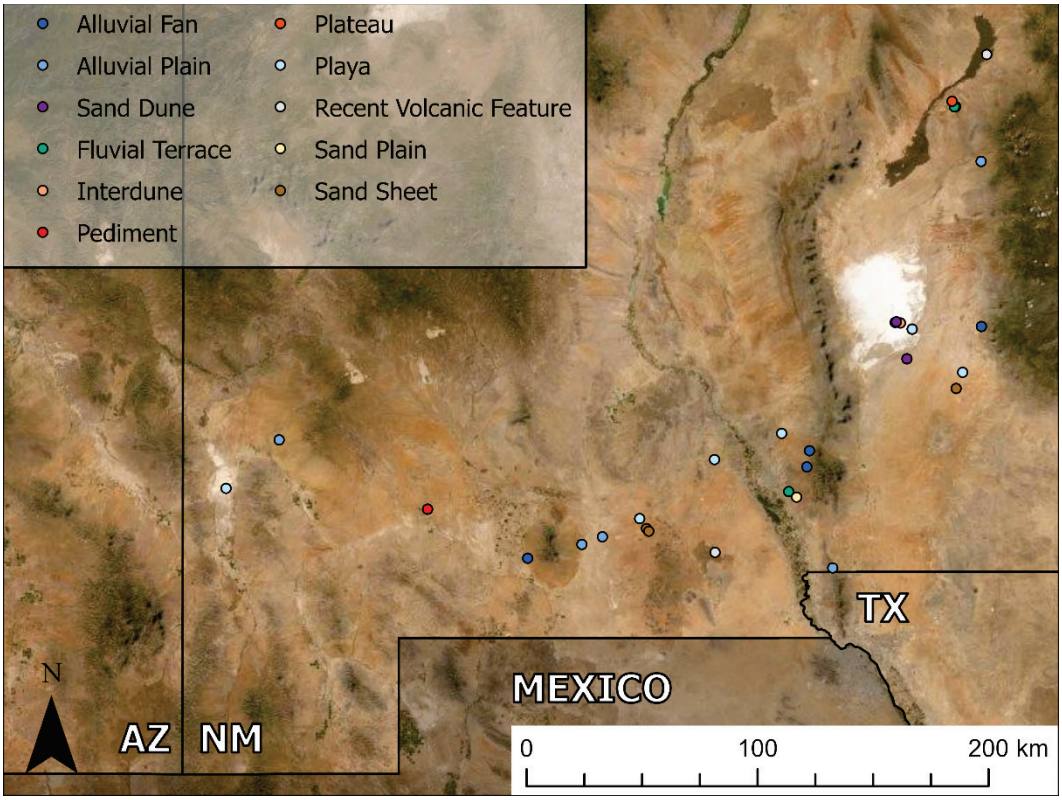

We separated the 11 landform types into three groupings, predominantly based on their geomorphic commonalities. The first group contains aeolian (i.e., wind-shaped) sand features, including sand dunes, interdunes, sand sheets, and sand plains (Table 2). The second group contains fluvial features (i.e., features formed by flowing water), including alluvial fans, alluvial plains, fluvial terraces, and playas (Table 3). The third group contains all other landform types considered, including plateaus, recent volcanic features, and pediments (Table 4).

Table 2. Group 1: sand feature landform data. Asterisks denote landform classifications deemed incorrect by the field team. The field team's suggested landform type is listed in parentheses beneath each incorrect classification. Latitude and longitude are reported in decimal degrees (DD).

Site ID	Date & Time	Weather (°F)	Landform Type	Waypoint Location	Latitude (DD)	Longitude (DD)	Elevation (m)	Notes
07-08-03	7/8/21 10:33	Sunny, cloud cover 3%, 81°	Sand dune	Center	32.8216	−106.2729	1,211.45	0% vegetation cover. Soil: white sand, no crusting present. Disturbance: light human foot traffic.
06-24-06	6/24/21 16:42	Sunny, cloud cover 50%	Sand dune* (Hill)	~300 m north	32.7009	−106.232	1,214.08	50% vegetation cover (*Bouteloua eriopoda* grassland). Soil: white-brown, calcareous sandy loam. No visible disturbance. Landform located on a military installation and inaccessible.
07-08-01	7/8/21 9:36	Sunny, cloud cover 1%, 79°	Interdune	Center	32.8182	−106.2575	1,203.69	25% vegetation cover (*Achnatherum hymenoides*, *Abronia sp.*, *Ephedra sp.*, *Yucca angustissima*, *Yucca schidigera*). Soil: white sand (gypsum), biocrust present. Disturbance: light foot traffic.
07-08-02	7/8/21 10:10	Sunny, cloud cover 2%	Interdune	Northern end	32.8194	−106.2775	1,210.83	5% vegetation cover (*Achnatherum hymenoides*, *Abronia sp.*). Soil: white sand, physical crusting present. Disturbance: light human foot traffic.
07-08-05	7/8/21 12:17	Sunny, cloud cover 10%, 84°	Sand sheet	Center	32.6037	−106.0400	1,225.83	25% vegetation cover (*Prosopis glandulosa*, *Atriplex canescens*, *Yucca angustissima*, *Yucca schidigera*). Soil: red sand. Disturbance: moderate cattle signs.
07-14-04	7/14/21 12:30	Sunny, cloud cover 35%, 90°	Sand sheet	Center	32.1437	−107.2449	1,288.01	30% vegetation cover (*Prosopis glandulosa*, *Ephedra sp.*). Soil: reddish brown sandy clay, some physical crusting. Disturbance: heavy cow use.
07-14-05	7/14/21 13:08	Sunny, cloud cover 35%, 90°	Sand sheet	Center	32.1355	−107.2360	1,283.22	15% vegetation cover (*Prosopis glandulosa*). Soil: reddish brown sandy loam, some physical crusting. Disturbance: heavy cow use.
06-25-01	6/25/21 8:45	Sunny, cloud cover 0%	Sand plain	Northern end	32.2473	−106.6609	1,312.24	20% vegetation cover (*Larrea tridentata*, *Ephedra sp.*, *Yucca schidigera*, *Gutierrezia sarothrae*, *Sporobolus sp.*). Soil: Red sand. Disturbance: Power line right of way and road along northern edge of feature, very old cattle sign.

Table 3. Group 2: fluvial feature landform data. Asterisks denote landform classifications deemed incorrect by the field team. The field team's suggested landform type is listed in parentheses beneath each incorrect classification.

Site ID	Date & Time	Weather (°F)	Landform Type	Waypoint Location	Latitude (DD)	Longitude (DD)	Elevation (m)	Notes
07-10-05	7/10/21 14:50	Sunny, 99°	Alluvial fan	Western edge	32.0462	−107.707	1,276.74	25% vegetation cover (*Prosopis glandulosa*, *Gutierrezia sarothrae*, *Atriplex canescens*). Soil: red sandy, gravelly. Disturbance: no visible anthropogenic disturbance.
06-25-03	6/25/21 11:21	Sunny, cloud cover 3%, 91°	Alluvial fan	Center	32.3470	−106.6216	1,532.086	20% vegetation cover (*Prosopis glandulosa*, *Gutierrezia sarothrae*, *Ephedra sp.*). Soil: Red loamy sand; gravelly. Disturbance: heavy cattle.
06-25-04	6/25/21 12:00	Sunny, cloud cover 5%, 93°	Alluvial fan	~400 m west of center	32.3998	−106.6103	1,526.18	35% vegetation cover (*Larrea tridentata*, *Prosopis glandulosa*, *Yucca schidigera*, *Ephedra sp.*, *Gutierrezia sarothrae*, unknown perennial grass). Soil: red-brown loamy sand; gravelly, cobbly; boulders present. Disturbance: Heavy cattle (grasses heavily grazed).
06-28-01	6/28/21 8:45	Light rain, cloud cover 98%, 64°	Alluvial fan	Center	32.8063	−105.9419	1,292.50	55% vegetation cover (*Prosopis glandulosa*, *Fallugia paradoxa*, *Opuntia sp.*, *Larrea tridentata*, *Yucca spp.*). Soil: gray-brown (moist color) sand, gravelly, cobbles. Disturbance: no visible anthropogenic disturbance.
07-10-02	7/10/21 11:06	Sunny, cloud cover 1%, 86°	Alluvial plain	180 m southeast of center	32.4351	−108.674	1,365.64	15% vegetation cover (*Gutierrezia sarothrae*, *Yucca schidigera*, *Ephedra sp.*, *Cylindropuntia imbricata*). Soil: light brown sand, gravelly. Disturbance: heavy cattle signs.
06-24-05	6/24/21 14:37	Sunny, cloud cover 30%, 93°	Alluvial plain	Center	33.3431	−105.943	1,681.41	45% vegetation cover (*Prosopis glandulosa/Gutierrezia sarothrae* shrubland). Soil: Red-brown sandy loam. Disturbance: heavy cattle signs.
06-28-02	6/28/21 10:24	Light rain, cloud cover 100%, 63°	Alluvial plain	400 m southeast of center	32.0145	−106.5208	1,336.07	50% vegetation cover (*Larrea tridentata*, *Yucca schidigera*, *Opuntia sp.*, *Echinocereus dasyacanthus*, *Yucca sp.*). Soil: light brown (moist) loamy sand. Disturbance: unpaved road through landform, cattle signs, *L. tridentata* water-stressed.
07-15-02	7/15/21 10:04	Sunny, light wind, cloud cover 10%	Alluvial plain	Center	32.5414	−106.8259	1,325.40	25% vegetation cover (*Prosopis glandulosa*, *Gutierrezia sarothrae*, *Atriplex canescens*, *Amaranthus sp.*). Soil: red-brown loamy sand. Disturbance: heavy cattle sign.
07-14-01	7/14/21 8:00	Sunny, cloud cover 0%, 75°	Alluvial plain	Center	32.1172	−107.4159	1,241.02	45% vegetation cover (*Acacia sp.*). Soil: reddish brown sandy loam, no crusting present. Disturbance: heavy cow use.
07-14-02	7/14/21 9:00	Sunny, cloud cover 10%, 81°	Alluvial plain	Center	32.0922	−107.4959	1,232.94	95% vegetation cover (*Tobosa sp.*, *Prosopis glandulosa*). Soil: gray-brown clay loam, physical crust present.

Table 3 (cont.). Group 2: fluvial feature landform data. Asterisks denote landform classifications deemed incorrect by the field team. The field team's suggested landform type is listed in parentheses beneath each incorrect classification.

Site ID	Date & Time	Weather (°F)	Landform Type	Waypoint Location	Latitude (DD)	Longitude (DD)	Elevation (m)	Notes
06-24-02	6/24/21 11:05	Sunny, cloud cover 10%, 87°	Fluvial terrace	Center	33.5214	−106.043	1,524.55	25% vegetation cover (*Larrea tridentata*/*Prosopis glandulosa* shrubland). Soil: light gray-brown, sandy/gravelly. Disturbance: Heavy cattle sign, possible herbicide treatment (numerous dead shrubs).
06-24-03	6/24/21 11:32	Sunny, cloud cover 25%, 87°	Fluvial terrace	Center	33.5205	−106.047	1,518.83	30% vegetation cover (grassy shrubland, *Larrea tridentata*, *Salsola sp.*). Soil: light gray-brown, sandy/gravelly. Disturbance: Heavy cattle sign, non-native plant invasion (*Salsola sp.*). Other notes: calcareous clay uplands located nearby.
06-25-02	6/25/21 10:24	Sunny, cloud cover 2%, 90°	Fluvial terrace* (flood plain or alluvial plain)	Center	32.2659	−106.6912	1,271.12	25% vegetation cover (*Larrea tridentata*, *Prosopis glandulosa*, *Fouquieria splendens*, *Cylindropuntia leptocaulis*). Soil: light brown, loamy sand. Disturbance: signs of occasional flooding (i.e., drainage channels).
07-08-04	7/08/21 11:01	Sunny, cloud cover 3%	Playa	~400 m southwest of center	32.7978	−106.2118	1,212.11	1% vegetation cover (*Atriplex canescens*, *Allenrolfea occidentalis*). Soil: light brown sand at playa margin, light brown loamy sand in playa floor, salt crusting present. Disturbance: light foot traffic.
07-08-06	7/08/21 13:30	Sunny, cloud cover 18%	Playa	Northeast edge	32.6565	−106.0149	1,218.25	35% vegetation cover (*Atriplex canescens*, *Bouteloua sp.*, *Chamaesyce sp.*, *Gutierrezia sarothrae*). Soil: light brown sandy clay loam. Disturbance: heavy cattle sign.
07-09-01	7/09/21 7:59	Sunny, recent rain, cloud cover 0%, 77°	Playa	Center	32.3706	−106.9802	1,348.75	55% vegetation cover (unknown annual grasses and forbs). Soil: red-brown (moist) clay. Disturbance: heavy cattle signs.
07-10-03	7/10/21 12:10	Sunny, cloud cover 20%, 101°	Playa	Center	32.2766	−108.88	1,264.73	15% vegetation cover (unidentified perennial grasses, *Atriplex canescens*). Soil: white-brown clay. Disturbance: roadways and railroad tracks through feature, cattle sign.
07-15-01	7/15/21 8:17	Sunny, light wind, cloud cover 10%	Playa	Center	32.4564	−106.719	1,303.28	2% vegetation cover (*Malvaceae sp.*). Soil: medium brown sandy clay loam with saline precipitate. Disturbance: heavy cattle sign.
07-14-03	7/14/21 11:17	Sunny, cloud cover 25%, 88°	Playa	Center	32.1764	−107.2717	1,273.63	20% vegetation cover (*Prosopis glandulosa*, *Larrea tridentata*). Soil: whitish brown sandy clay, physical crust present. Disturbance: light cow use.

Table 4. Group 3: all other features landform data. Asterisks denote landform classifications deemed incorrect by the field team. The field team's suggested landform type is listed in parentheses beneath each incorrect classification.

Site ID	Date & Time	Weather (°F)	Landform Type	Waypoint Location	Latitude (DD)	Longitude (DD)	Elevation (m)	Notes
06-24-04	6/24/21 12:32	Sunny, cloud cover 18%, 91°	Plateau	Center	33.5385	−106.056	1,529.62	30% vegetation cover (succulent shrubland: *Larrea tridentata*, *Prosopis glandulosa*, Mariola, *Yucca sp.*). Soil: loose red sand over light-brown physical crust. Disturbance: light cattle sign.
06-24-01	6/24/21 9:30	Sunny, cloud cover 5%, 82°	Recent volcanic feature	Center	33.6893	−105.922	1,601.34	20% vegetation cover (succulent shrubland). Soil: light gray-brown sandy loam. Disturbance: road through feature, state park infrastructure located in feature.
07-14-06	7/14/21 15:07	Sunny, cloud cover 10%, 95°	Recent volcanic feature	~1 mile northeast	32.0657	−106.9784	1,290.24	25% vegetation cover (*Flourensia cernua*). Soil: black basalt with reddish brown sandy loam in interspaces. Disturbance: light human use and heavy cow use in periphery of outcrop.
07-10-04	7/10/21 13:41	Sunny, cloud cover 15%, 97°	Pediment* (Alluvial plain)	Center	32.2077	−108.096	1,359.13	30% vegetation cover (*Larrea tridentata*). Soil: medium brown loamy sand, gravelly. Disturbance: light cattle sign.

3.2 Remote mapping results

Satellite imagery was reviewed and interpreted; as a result, 97 site locations and 15 landform types were identified (Figure 4). In total, analysts remotely mapped 1 sand dune, 4 sand sheets, 9 alluvial fans, 2 alluvial plains, 4 fluvial terraces, 9 playas, 13 plateaus, 2 pediments, 1 badlands, 13 agriculture, 11 bedrock, 8 fine-grained lake deposits, 10 urban, 9 water, and 1 wind erosional feature. Table 5 lists each of these landforms, the mapper's confidence level in the suggested classification, and comments that provide context for the chosen confidence level.

Figure 4. Overview of all remotely identified landform locations in Mexico, New Mexico, and Texas; 15 landform types were identified at 97 field sites. The 97 landform sites are shown as *color-categorized circles*.

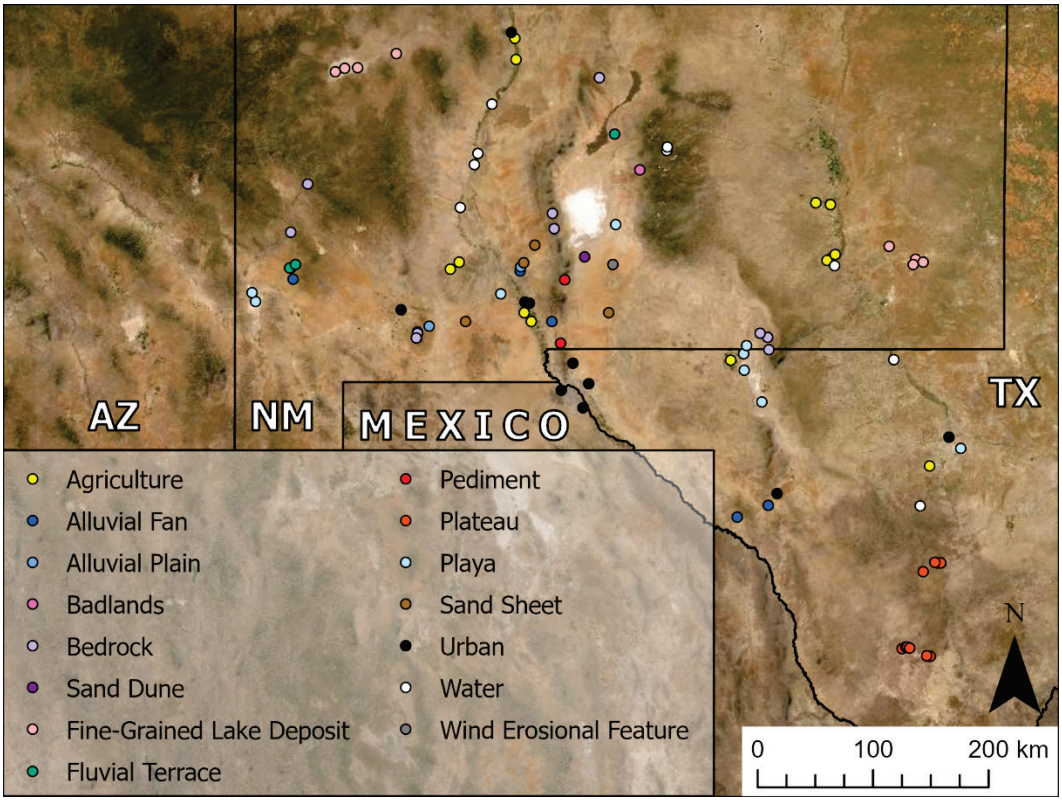

Table 5. All landforms identified through remote satellite interpretation. The confidence level associated with each landform site expresses the mapper's confidence in each classification. A high level of confidence was assigned to features with a classic geomorphic expression, meaning the landforms had easily identifiable characteristics. Sand sheets and sand plains could not be differentiated from one another using satellite imagery alone, but they could be classified as either/or with a high degree of certainty. Therefore, the high level of confidence assigned to the sand sheets and sand plains, as noted with an asterisk, represents confidence that the landform is one of those two landform types.

Landform Identified Remotely	Latitude (DD)	Longitude (DD)	Confidence Level	Comments
Sand dune	32.6063	−106.33	Medium	Nondirectional; undulating pattern not clear; could be eroded or older sand dune field, interdunes, or scoured mounds
Playa	32.8174	−106.086	High	Classic geomorphic expression
Playa	32.3134	−108.888	High	Classic geomorphic expression
Playa	32.3706	−108.914	High	Classic geomorphic expression
Playa	31.3469	−103.403	High	Classic geomorphic expression
Playa	31.8613	−105.086	High	Classic geomorphic expression
Playa	31.6515	−104.948	High	Classic geomorphic expression
Playa	31.9704	−105.090	High	Classic geomorphic expression
Playa	32.0256	−105.067	High	Classic geomorphic expression
Playa	32.3643	−106.980	High	Classic geomorphic expression
Pediment	32.4579	−106.484	High	Two nearby erosional sources; slope looks apparent, but elevation change unknown
Pediment	32.0417	−106.516	Medium	Classic alluvial fan shape (lobed); distal from source; could be an alluvial fan—determination could not be made without elevation data
Wind erosional feature	32.5579	−106.108	Low	Feature directionality not clear; scoured surface; possible eroded or older sand dune field
Alluvial plain	32.5414	−106.826	High	Point is offset 200 m northwest of landform that has a markedly different sedimentology (dark gray); flow lines observable
Alluvial plain	32.1519	−107.538	High	Point located on distal lobe of feature; channeling observable in imagery
Sand sheet	32.2429	−106.143	High*	Sand sheet or sand plain; determination cannot be made without in situ observations
Sand sheet	32.6849	−106.717	High*	Sand sheet or sand plain; determination cannot be made without in situ observations

Table 5 (cont.). All landforms identified through remote satellite interpretation. The confidence level associated with each landform site expresses the mapper's confidence in each classification. A high level of confidence was assigned to features with a classic geomorphic expression, meaning the landforms had easily identifiable characteristics. Sand sheets and sand plains could not be differentiated from one another using satellite imagery alone, but they could be classified as either/or with a high degree of certainty. Therefore, the high level of confidence assigned to the sand sheets and sand plains, as noted with an asterisk, represents confidence that the landform is one of those two landform types.

Landform Identified Remotely	Latitude (DD)	Longitude (DD)	Confidence Level	Comments
Sand sheet	32.5682	−106.803	High*	Sand sheet or sand plain; determination cannot be made without in situ observations
Sand sheet	32.1813	−107.253	High*	Sand sheet or sand plain; determination cannot be made without in situ observations; unique mineralogy (color) likely sourced from eroding evaporates from western feature
Fluvial terrace	33.4085	−106.095	High	Large channel system observed; elevation changes unknown
Fluvial terrace	32.5327	−108.615	Medium	Point appears 70 m east of actual feature; could be result of poor georectification; nearby channel clearly observable
Fluvial terrace	32.5345	−108.622	Low	Partially obscured by cloud coverage; point is due west of actual feature; point is located on a ridge
Fluvial terrace	32.5566	−108.578	Medium	Point appears 50 m east of actual feature; could be a result of poor georectification; zooming out, river valley is apparent
Badlands	33.1726	−105.897	Low	Erosional characteristics present; apparent sedimentological banding; field team drove by this region and confirmed from a distance that this point is a cliff
Plateau	29.9607	−103.5924	High	Classic geomorphic expression
Plateau	29.9957	−103.6086	High	Classic geomorphic expression
Plateau	30.0217	−103.5358	High	Classic geomorphic expression
Plateau	30.0063	−103.861	High	Classic geomorphic expression
Plateau	30.0177	−103.832	High	Classic geomorphic expression
Plateau	30.0183	−103.819	High	Classic geomorphic expression
Plateau	30.0119	−103.801	High	Classic geomorphic expression
Plateau	29.9565	−103.640	High	Classic geomorphic expression
Plateau	29.9612	−103.667	High	Classic geomorphic expression
Plateau	30.5244	−103.694	High	Classic geomorphic expression
Plateau	30.5803	−103.581	High	Classic geomorphic expression
Plateau	30.5835	−103.558	High	Classic geomorphic expression

Table 5 (cont.). All landforms identified through remote satellite interpretation. The confidence level associated with each landform site expresses the mapper's confidence in each classification. A high level of confidence was assigned to features with a classic geomorphic expression, meaning the landforms had easily identifiable characteristics. Sand sheets and sand plains could not be differentiated from one another using satellite imagery alone, but they could be classified as either/or with a high degree of certainty. Therefore, the high level of confidence assigned to the sand sheets and sand plains, as noted with an asterisk, represents confidence that the landform is one of those two landform types.

Landform Identified Remotely	Latitude (DD)	Longitude (DD)	Confidence Level	Comments
Plateau	30.5841	−103.602	High	Classic geomorphic expression
Alluvial fan	32.4592	−108.597	High	Classic geomorphic expression
Alluvial fan	32.5135	−106.83	Medium	Classic fan shape not expressed; could be caused by small hill diverting sediment; likely a fan but uncertain due to lack of typical lobe expression; could be pediments
Alluvial fan	30.9926	−105.0395	High	Classic geomorphic expression
Alluvial fan	30.9312	−104.9850	High	Classic geomorphic expression
Alluvial fan	29.8824	−103.6466	High	Classic geomorphic expression
Alluvial fan	29.8966	−103.6733	High	Classic geomorphic expression
Alluvial fan	30.8878	−105.144	High	Classic geomorphic expression
Alluvial fan	32.1835	−106.586	High	Classic geomorphic expression
Alluvial fan	30.9668	−104.901	High	Classic geomorphic expression
Agriculture	32.5966	−104.415	High	Classic geomorphic expression
Agriculture	32.5831	−104.444	High	Classic geomorphic expression
Agriculture	32.6206	−104.380	High	Classic geomorphic expression
Agriculture	32.9484	−104.417	High	Classic geomorphic expression
Agriculture	32.9592	−104.529	High	Classic geomorphic expression
Agriculture	31.9269	−105.192	High	Classic geomorphic expression
Agriculture	31.2270	−103.645	High	Classic geomorphic expression
Agriculture	33.8890	−106.861	High	Classic geomorphic expression
Agriculture	34.0259	−106.872	High	Classic geomorphic expression
Agriculture	32.5245	−107.373	High	Classic geomorphic expression
Agriculture	32.5724	−107.304	High	Classic geomorphic expression
Agriculture	32.1826	−106.744	High	Classic geomorphic expression
Agriculture	32.2428	−106.799	High	Classic geomorphic expression
Fine-grained lake deposit	33.8086	−108.268	High	Classic geomorphic expression
Fine-grained lake deposit	33.8329	−108.194	High	Classic geomorphic expression

Table 5 (cont.). All landforms identified through remote satellite interpretation. The confidence level associated with each landform site expresses the mapper's confidence in each classification. A high level of confidence was assigned to features with a classic geomorphic expression, meaning the landforms had easily identifiable characteristics. Sand sheets and sand plains could not be differentiated from one another using satellite imagery alone, but they could be classified as either/or with a high degree of certainty. Therefore, the high level of confidence assigned to the sand sheets and sand plains, as noted with an asterisk, represents confidence that the landform is one of those two landform types.

Landform Identified Remotely	Latitude (DD)	Longitude (DD)	Confidence Level	Comments
Fine-grained lake deposit	33.8372	−108.093	High	Classic geomorphic expression
Fine-grained lake deposit	33.9267	−107.791	High	Classic geomorphic expression
Fine-grained lake deposit	32.5933	−103.753	High	Classic geomorphic expression
Fine-grained lake deposit	32.5713	−103.696	High	Classic geomorphic expression
Fine-grained lake deposit	32.5563	−103.773	High	Classic geomorphic expression
Fine-grained lake deposit	32.6751	−103.961	High	Classic geomorphic expression
Bedrock	32.7900	−106.566	High	Mountain ridge, little to no vegetation cover
Bedrock	32.8904	−106.580	High	Mountain ridge, little to no vegetation cover
Bedrock	32.7685	−108.614	Medium	Mountain ridge, vegetation on opposite slope
Bedrock	33.0840	−108.482	Medium	Mountain slope, sparse vegetation
Bedrock	31.9977	−104.898	High	Classic geomorphic expression, bedding exposed
Bedrock	32.0779	−104.904	High	Classic geomorphic expression, bedding exposed
Bedrock	32.1056	−104.966	High	Classic geomorphic expression, bedding exposed
Bedrock	33.7722	−106.217	High	Bedding exposed, sparse vegetation
Bedrock	32.1128	−107.630	High	Ridge top, bedding exposed
Bedrock	32.1073	−107.628	High	High relief, bedding exposed
Bedrock	32.0733	−1076379	High	High relief, bedding exposed
Water	31.9332	−103.924	High	Classic geomorphic expression
Water	32.5497	−104.383	High	Classic geomorphic expression
Water	33.2083	−107.188	High	Classic geomorphic expression
Water	33.2821	−107.161	High	Classic geomorphic expression
Water	32.9309	−107.298	High	Classic geomorphic expression
Water	30.9634	−103.719	High	Classic geomorphic expression

Table 5 (cont.). All landforms identified through remote satellite interpretation. The confidence level associated with each landform site expresses the mapper's confidence in each classification. A high level of confidence was assigned to features with a classic geomorphic expression, meaning the landforms had easily identifiable characteristics. Sand sheets and sand plains could not be differentiated from one another using satellite imagery alone, but they could be classified as either/or with a high degree of certainty. Therefore, the high level of confidence assigned to the sand sheets and sand plains, as noted with an asterisk, represents confidence that the landform is one of those two landform types.

Landform Identified Remotely	Latitude (DD)	Longitude (DD)	Confidence Level	Comments
Water	33.2985	−105.688	High	Classic geomorphic expression
Water	33.3216	−105.686	High	Classic geomorphic expression
Water	33.5991	−107.048	High	Classic geomorphic expression
Urban	31.7317	−106.509	High	Classic geomorphic expression
Urban	31.7738	−106.295	High	Classic geomorphic expression
Urban	31.9097	−106.420	High	Classic geomorphic expression
Urban	31.6152	−106.343	High	Classic geomorphic expression
Urban	32.3018	−106.757	High	Classic geomorphic expression
Urban	32.3115	−106.792	High	Classic geomorphic expression
Urban	31.4206	−103.496	High	Classic geomorphic expression
Urban	31.0441	−104.832	High	Classic geomorphic expression
Urban	32.2587	−107.758	High	Classic geomorphic expression
Urban	34.0651	−106.901	High	Classic geomorphic expression

3.3 Individual landform type results

Sections 3.3.1 to 3.3.18 provide a summary of our results, broken down by landform type and including information learned through both in situ and remote methodologies. In instances in which we have field observations for a given landform type, we provide photos of the general surroundings. For the landform classes limited to remote identification, we provide satellite image examples.

3.3.1 Sand dune

We collected data at three sand dune field sites: two of these sites were assessed in the field, and one was assessed remotely. Of the two sand dunes mapped in the field, one location was a sand dune made out of white gypsum, which is a rather rare sedimentology, with 0% vegetation coverage (Figure 5). The other sand dune had roughly 50% vegetation coverage. The field team deemed this second location to be misclassified and instead suggested that a hill classification more appropriately described the landform

type. However, this particular site could also have been a dormant, grass-covered sand dune.

Figure 5. Overview photo of a gypsum sand dune observed by the field team.

The remotely mapped sand dune location displayed some level of directionality and undulation typical of a dune field; however, it did not exhibit a regular, repeating landform structure as expected (Figure 6). It is unclear if the location of the actual marked point shown in the top panel of Figure 6 represents a sand dune; it could potentially be an interdune or an older, stabilized dune with potential ponding surrounding it. For these reasons, we labeled this site as a sand dune with a medium confidence level.

Figure 6. *Top*: Satellite image of a remotely mapped sand dune location. The *yellow circle* represents the actual field site for this landform. *Bottom*: Satellite image of a dune field that depicts the regular, repeating, undulating structure typical of this landform type.

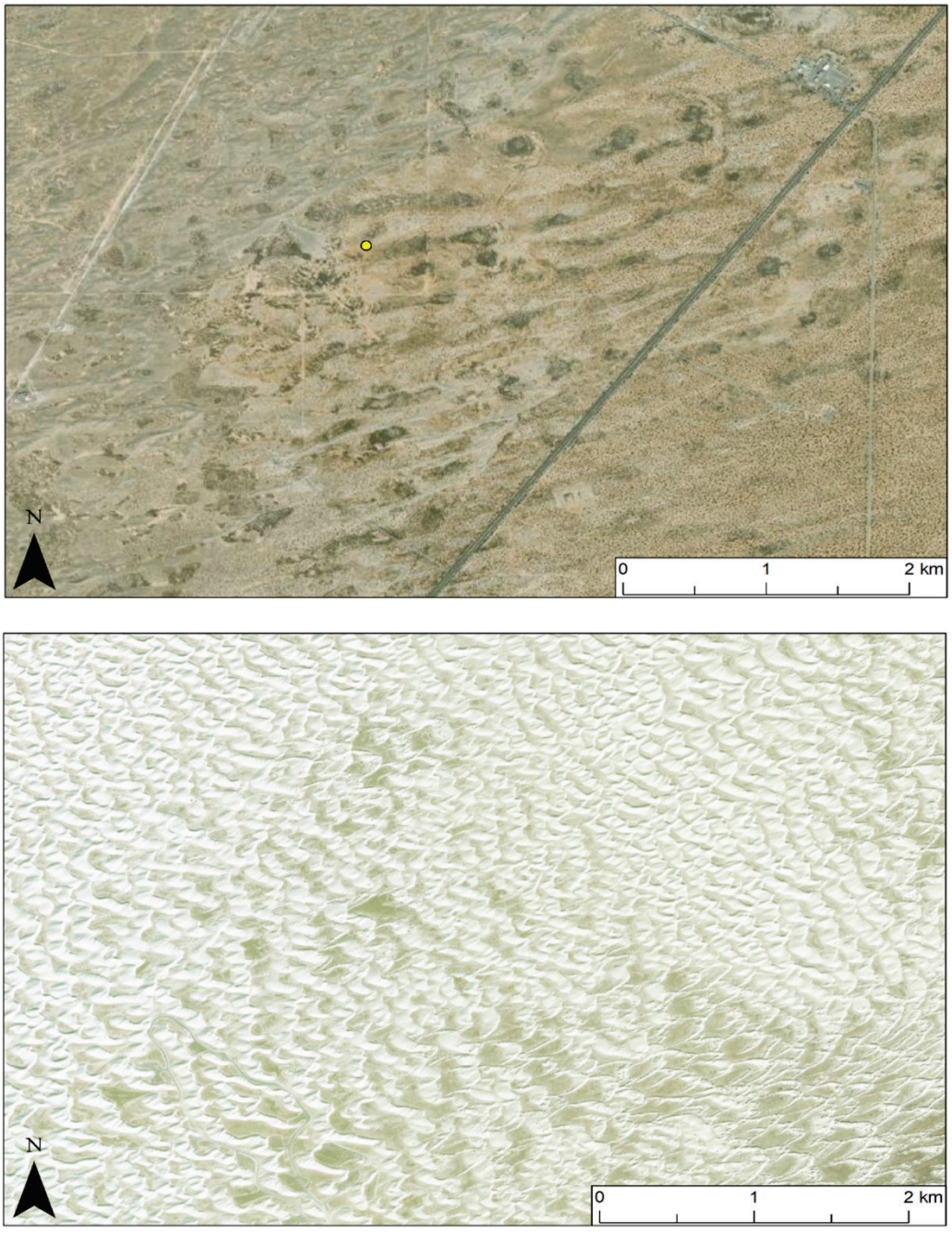

3.3.2 Interdune

The field team collected data at two interdune field sites (e.g., Figure 7), both of which had the same sedimentology as the sand dune site discussed

in the previous section (Figure 5). Vegetation coverage on the two interdunes ranged from 5% to 25%. The field team deemed both sites to be correctly classified. We did not map any interdune sites remotely.

Figure 7. Overview photo of a gypsum interdune observed by the field team.

3.3.3 Sand sheet

We collected data at seven sand sheet field sites; the field team visited three locations and mapped four sites remotely. For the in situ sites, vegetation coverage ranged from 15% to 30%, and two sites showed indications of physical crusting (Figure 8). The field team perceived all three sites to be correctly classified.

Figure 8. Overview photo of a sand sheet observed by the field team.

Analysts labeled all four of the remotely mapped sand sheets with a high level of confidence (Figure 9). However, we could not determine sand plains from sand sheets on satellite imagery because these two landform classes have very similar surface morphology. Therefore, the high confidence levels assigned to all four sand sheets represent the mapper's certainty that these sites are either a sand sheet or a sand plain.

Figure 9. Satellite image of a remotely mapped sand sheet location. The *yellow circle* represents the actual field site for this landform.

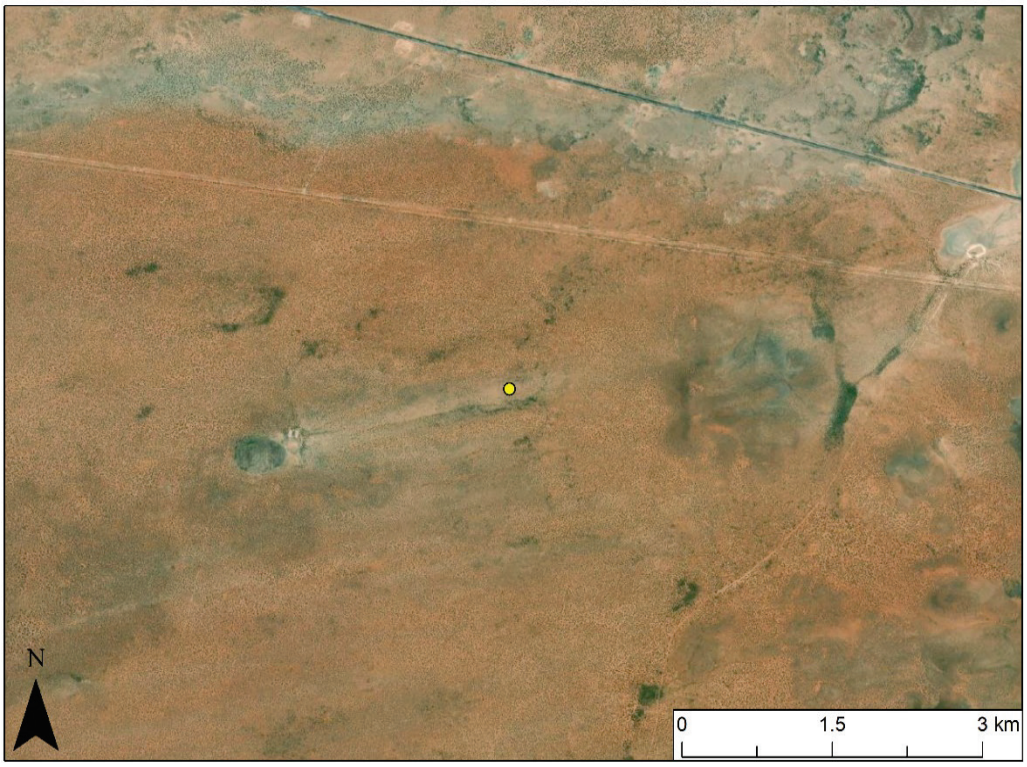

3.3.4 Sand plain

Due to a relative lack of sand plains in the field region, the field team was only able to collect data at one sand plain (Figure 10). There was approximately 20% vegetation coverage at this site, and the field team determined this location to be correctly classified. We did not map any sand plains remotely.

Figure 10. Overview photo of a sand plain observed by the field team.

3.3.5 Alluvial fan

We collected data at 13 alluvial fan field sites. The field team assessed four sites directly, and analysts mapped nine locations remotely. For the in situ sites, vegetation coverage ranged from 20% to 55%. The field team deemed all four in situ sites to be correctly classified (Figure 11).

Figure 11. Overview photo of an alluvial fan observed by the field team.

Eight of the nine remotely mapped alluvial fans were easily identified using remote mapping techniques, primarily due to the signature leaf-shaped morphology associated with alluvial fans (Figure 12). Analysts classified these areas with high confidence levels. One of the remotely mapped alluvial fans, however, did not display typical fan morphology (Figure 12,

bottom panel). The lack of a leaf shape at this location could be the result of a small rocky outcrop that appears to divert sediment. Because we were unable to make this determination with total certainty, analysts classified this ninth alluvial fan site with a medium confidence level.

Figure 12. Satellite images of two remotely mapped alluvial fans. The *yellow circles* represent the actual field site for each landform. *Bottom*: This remotely mapped alluvial fan does not display typical fan morphology, which may be caused by interference from the outcropping rocky knob (outlined by the *red rectangle*) located directly west of the yellow point.

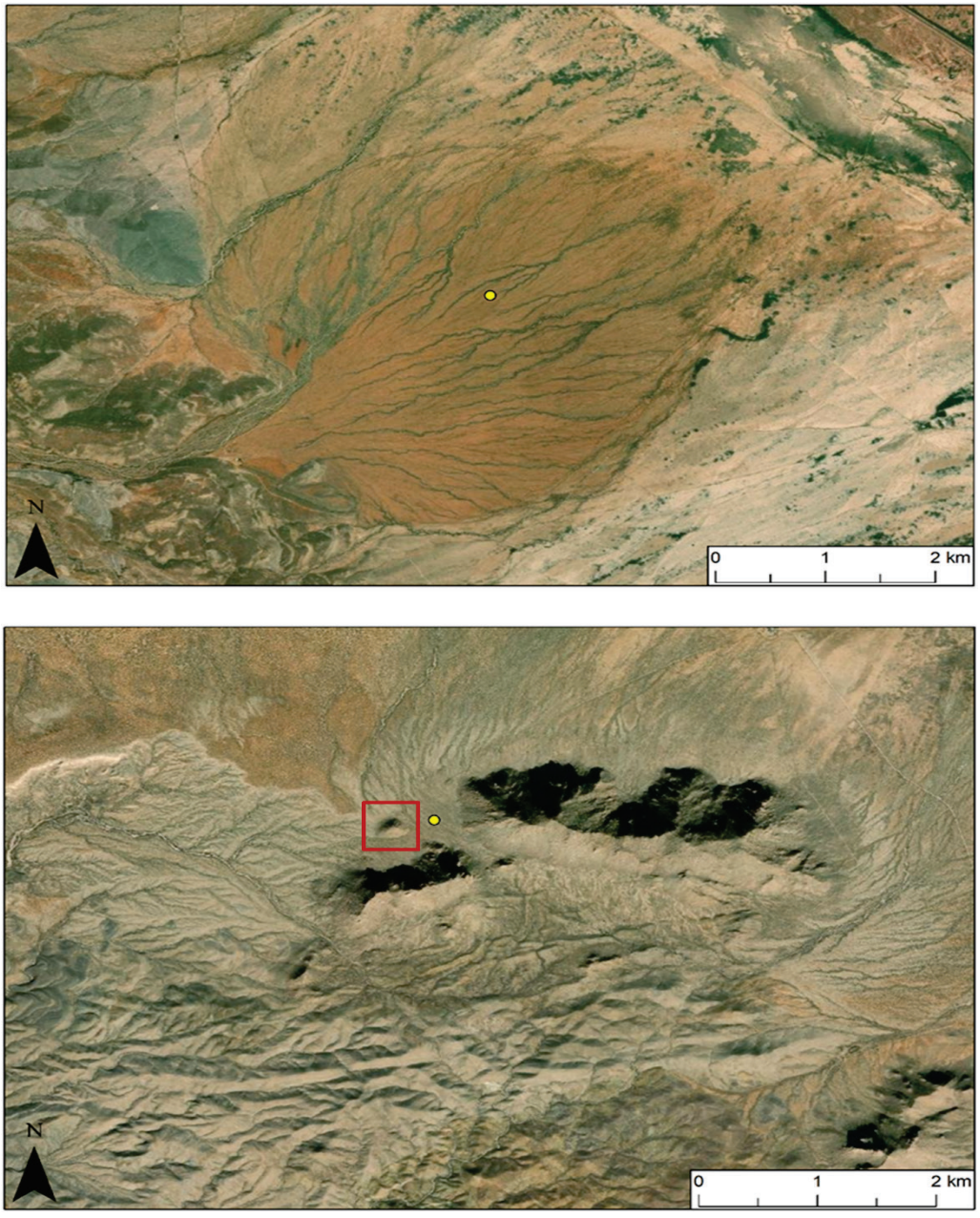

3.3.6 Alluvial plain

We collected data at eight alluvial plain field sites. The field team visited six sites, and analysts mapped two sites remotely. For the in situ sites, vegetation coverage ranged from 15% to 95%. Most of the in situ locations had experienced heavy disturbance by cattle or vehicle traffic. The field team deemed all six of the sites they visited to be correctly classified (Figure 13).

Figure 13. Overview photo of an alluvial plain observed by the field team.

Analysts classified both of the remotely mapped alluvial plains with high confidence levels. One of the geospatial data site markers that we consulted for guidance was approximately 200 m northwest of the actual landform, though the alluvial plain was clearly discernable. At the second location, the point marker was on the distal lobe of the landform (Figure 14). At both sites, however, analysts clearly observed visible flow patterns and, as such, recorded adjusted locations in the reference data set.

Figure 14. Satellite image of a remotely mapped alluvial plain location. The *yellow circle* represents the actual field site for this landform.

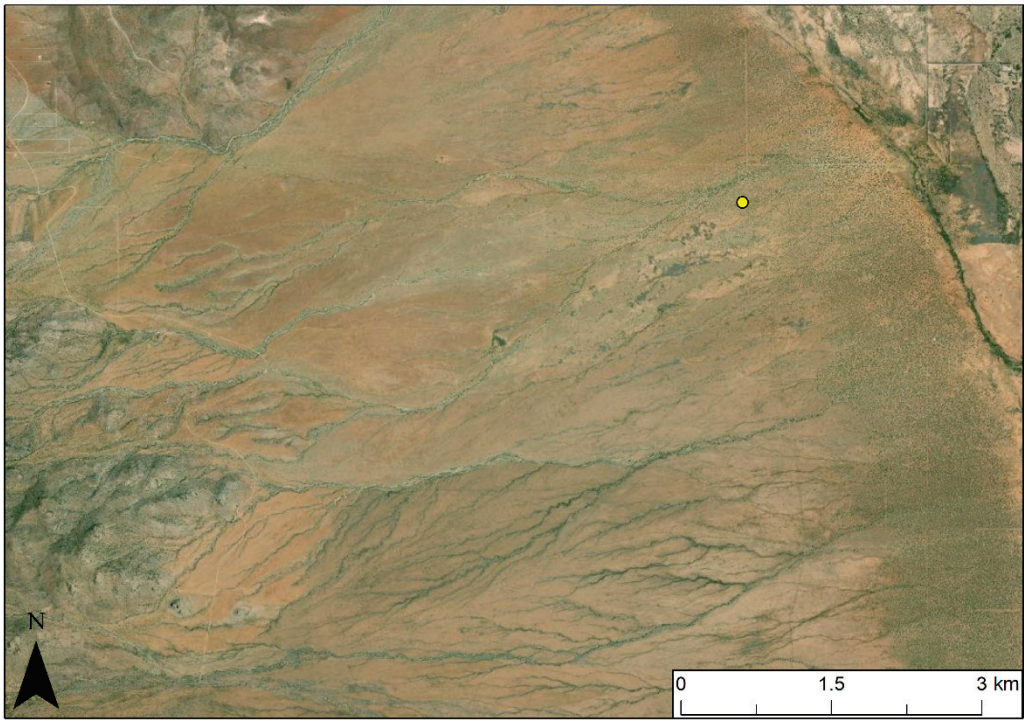

3.3.7 Fluvial terrace

We obtained data for seven fluvial terrace field sites; the field team visited three sites, and analysts mapped four locations remotely. For the in situ sites, vegetation coverage ranged from 25% to 30%, and two locations had signs of heavy disturbance by cattle (Figure 15). At one site, the field crew identified a change in sedimentology: a combination of chalky white sediment was near an area of light brown sand more typical of fluvial terraces in the region (Figure 15). The field team only perceived two of the three fluvial terrace sites to be correctly identified. The third site fit better as a flood plain or, potentially, an alluvial plain. Though both flood plains and fluvial terraces are formed by dynamic river-flow processes, fluvial terraces are elevated landforms that are shaped as water erodes materials away from their boundaries. Flood plains and alluvial plains occur in flatter, lower-elevation areas.

Figure 15. *Top*: Overview photo of a fluvial terrace observed by the field team. *Bottom*: Sedimentological changes noted on this fluvial terrace, which varied from light-colored chalky sediment to light-brown sand.

Analysts only classified one of the remotely mapped fluvial terraces with a high level of confidence, primarily because this location was near a large channel system (Figure 16). Two other fluvial terrace sites were labeled with a medium level of confidence. The guiding point markers for these sites seemed to be shifted east of the actual landform location by 50–70 m, which could potentially be a result of poor georectification in the geospatial data sets or a wide margin of error from the original GPS data collection (Figure 16, bottom panel). Analysts classified the fourth fluvial terrace with a low level of confidence because the location under consideration appeared to be a ridge. However, closer inspection of the imagery revealed that cloud cover partially obscured the basemap. To alleviate confusion,

the analysts performed supplemental assessments using Google Earth imagery and confirmed that the site in question was a ridge-like structure. Accordingly, the fourth site more closely aligned with the bedrock classification, rather than the fluvial terrace classification.

Figure 16. Satellite image of two remotely mapped fluvial terraces. The *yellow circles* represent the actual field sites for each landform, though the *yellow marker* in the bottom panel is estimated to be located approximately 50 m east of the true landform location.

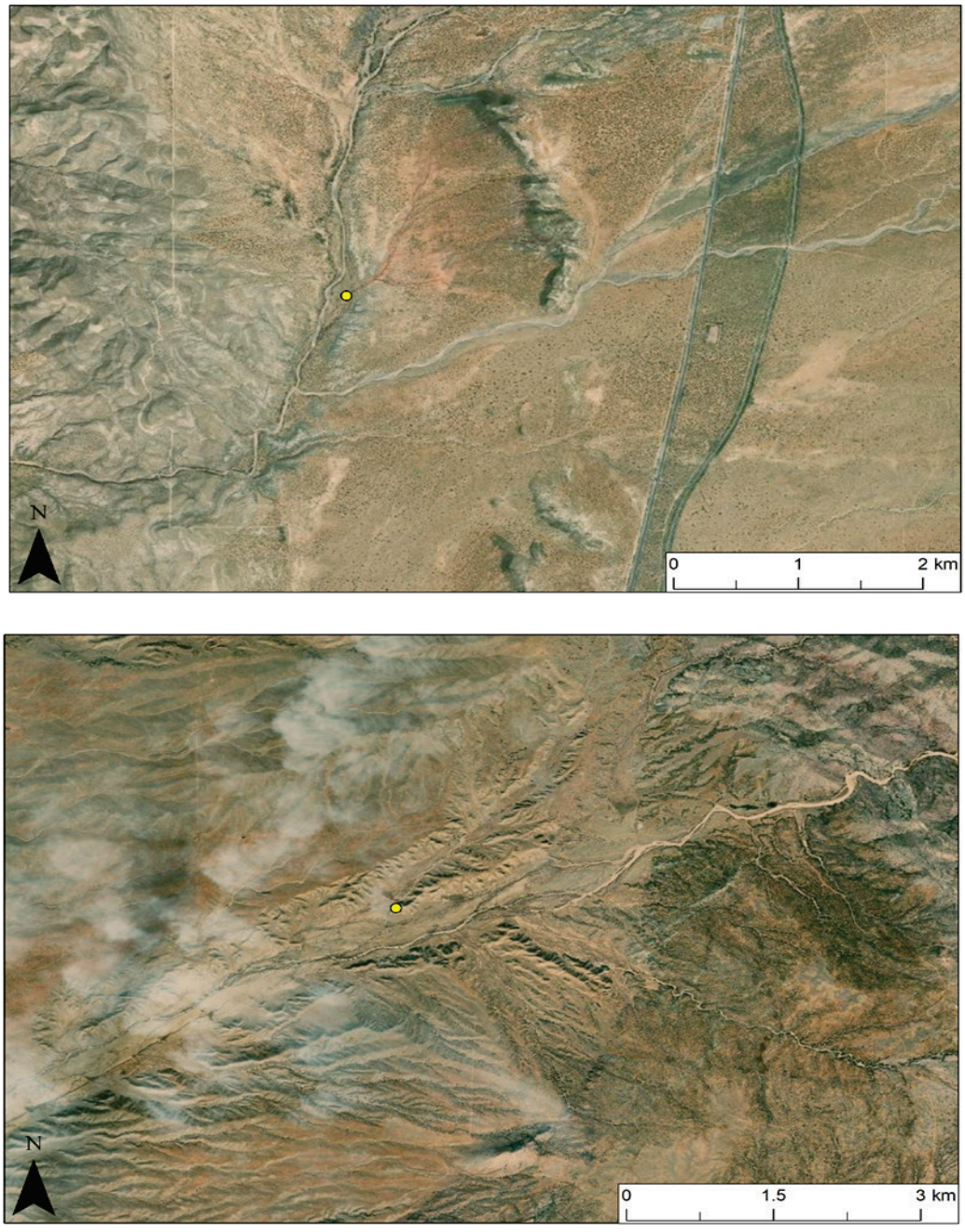

3.3.8 Playa

We collected data at 15 playa field sites; the field team assessed six locations on site, and analysts mapped nine remotely. For the in situ sites, vegetation coverage ranged from 1% to 55%. The field crew also noted soil crusting at two locations and heavy disturbance from cattle and vehicles at four locations (Figure 17). The field team deemed all in situ sites to be correctly classified.

Figure 17. Overview photo of a playa observed by the field team.

Analysts classified all nine of the remotely identified playas with a high level of confidence. This outcome was not surprising because playas are typically easy to distinguish based on their low levels of vegetation and flat-and-fine to sandy surface textures (Figure 18).

Figure 18. Satellite image of a remotely mapped playa field site. The *yellow circle* represents the actual location of this landform.

3.3.9 Plateau

We collected data for 14 plateau site locations; the field team sampled 1, and analysts mapped 13 sites remotely. The plateau inspected by the field team had 30% vegetation coverage and some minor surface disturbance (Figure 19). Researchers considered the site to be correctly classified.

Figure 19. Overview photo of a plateau observed by the field team.

The 13 additional remotely mapped plateaus were all located in Texas. As expected, the analysts classified all of these sites with high confidence levels because plateaus are easy to distinguish in satellite imagery due to their stark elevation contrasts (Figure 20).

Figure 20. Satellite image of a remotely mapped plateau field site. The *yellow circle* represents the actual location of this landform.

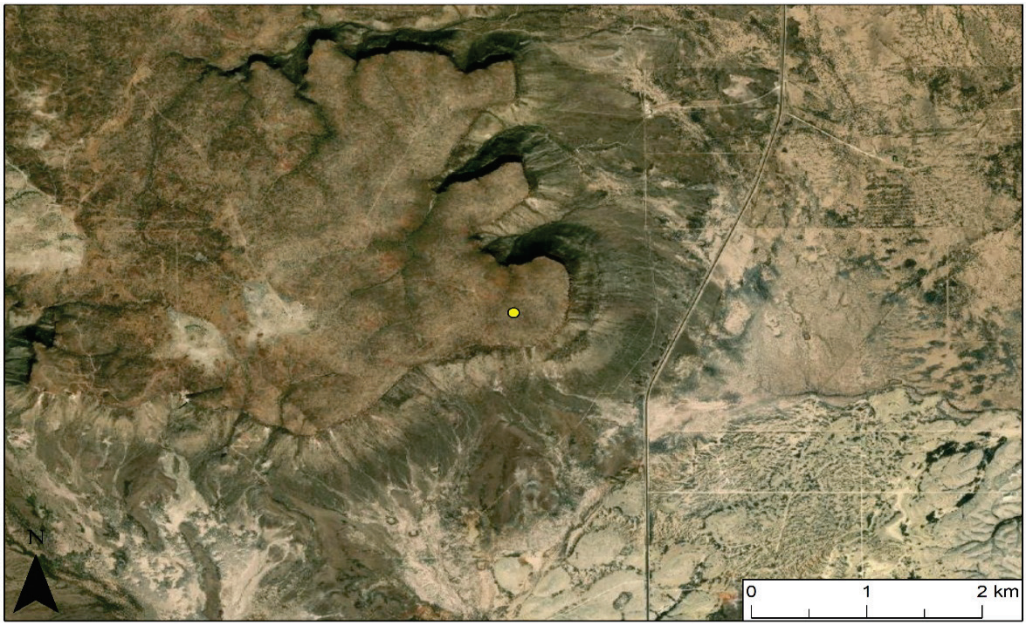

3.3.10 Recent volcanic feature

The field team inspected two recent volcanic features but did not map any additional sites remotely. Vegetation coverage between the two volcanic sites was similar, ranging between 20% and 25%. Due to the distinct dark, igneous volcanic rock composition, the field crew easily classified these locations (Figure 21).

Figure 21. Overview photo of a recent volcanic feature observed by the field team.

3.3.11 Pediment

We collected data at three pediment sites; the field team visited one location, and analysts mapped two remotely. The pediment assessed by the field team seemed misclassified. The crew suggested it was an alluvial plain, rather than a pediment (Figure 22).

Figure 22. Overview photo of a pediment field site that was observed by the field team and was interpreted and reclassified as an alluvial plain.

Analysts labeled one of the remotely mapped pediments with high confidence; they labeled the other potential pediment location with a medium level of confidence (Figure 23). The pediment marked with less certainty had a lobate, or leaf-shaped, morphology that is typical of an alluvial fan

(Figure 12) and could potentially indicate that this region would be more accurately described as an alluvial apron (i.e., a collection of overlapping alluvial fans). However, pediments can also have lobate expressions, so our analysts could not make a clear distinction between a lobed pediment and an alluvial fan at this site.

Figure 23. Satellite images of remotely mapped pediment field sites. The *yellow circles* represent the actual locations of each landform. *Bottom*: Pediment labeled with a medium level of confidence. The lobate or leaf shape of this landform suggests it could be an alluvial fan. Because a distinction between an alluvial fan and a pediment could not be made at this site, the confidence level was reduced to medium.

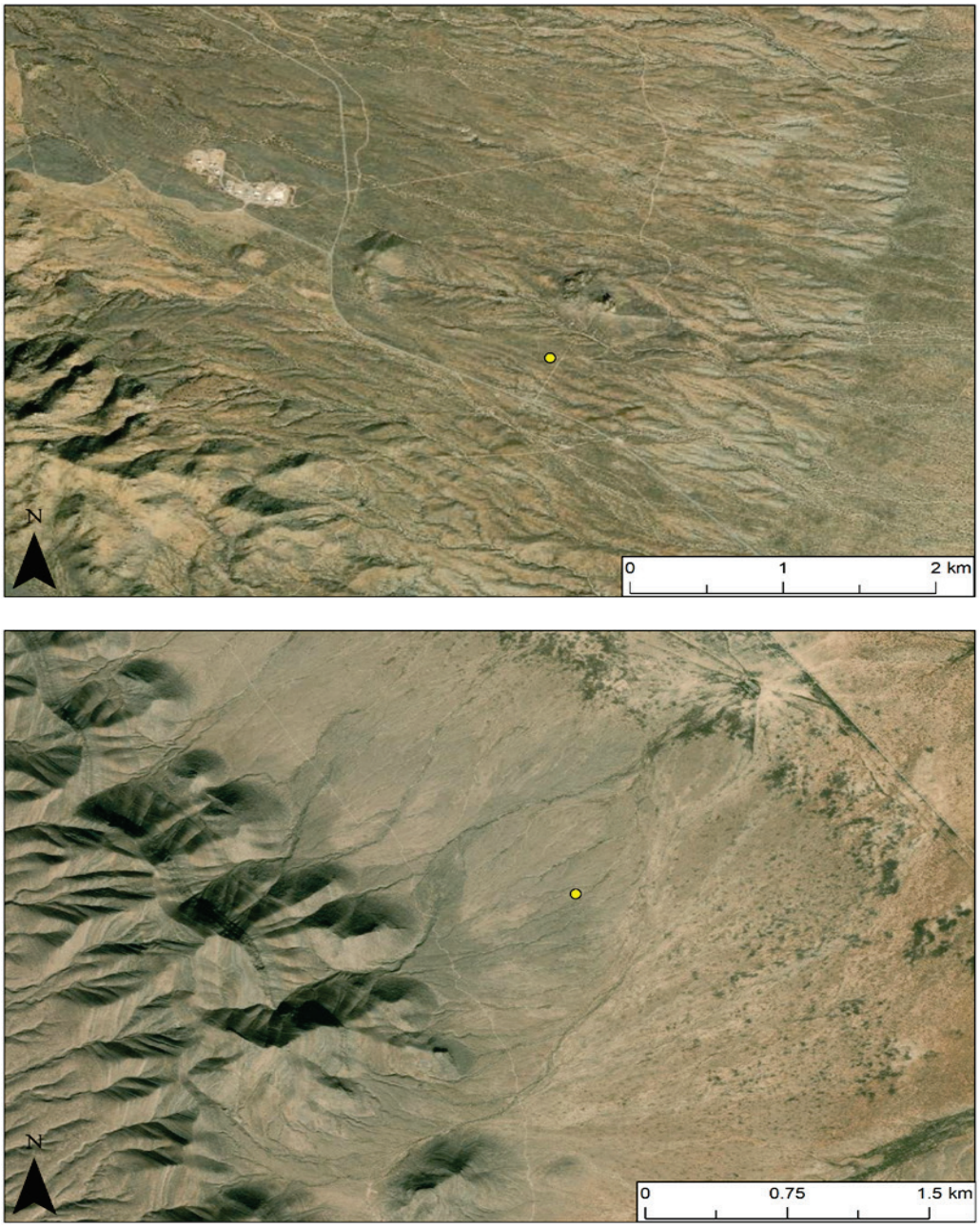

3.3.12 Badlands

We attempted to map a badlands site for this study, but analysts classified the one potential location we identified from guiding geospatial data sets with low confidence (Figure 24). Characteristics commonly associated with badlands, such as apparent erosional characteristics, banding, and a high-relief, were observable in the satellite imagery. However, the field team was able to assess this field site from a distance and determined it should be reclassified as a bedrock cliff because the site did not exhibit deep washes alternating with sharp narrow ridges, which is typical of badlands landforms.

Figure 24. Satellite image of a remotely identified badlands field site that was later determined to be misclassified. The *yellow circle* that represents the actual location for this landform was reclassified as a bedrock cliff by the field team. To see satellite imagery of an actual badlands site, see the Appendix.

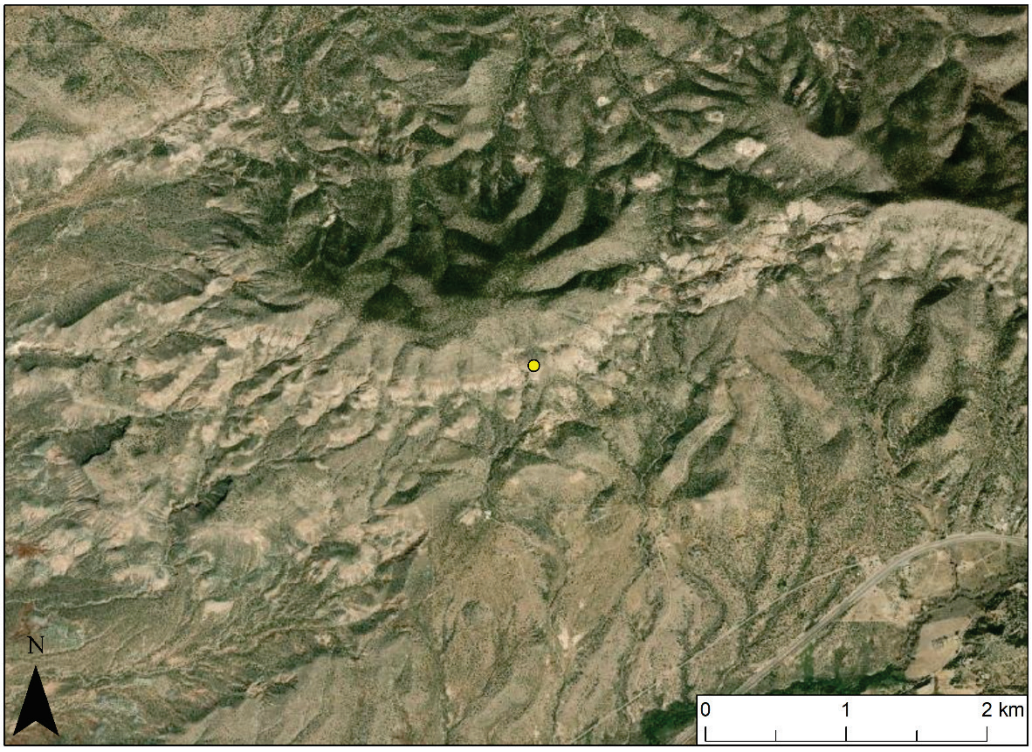

3.3.13 Wind erosional feature

We identified one wind erosional feature site through remote mapping. While there was an apparent wind-shaped directionality to the landform, the actual location of the point marker from the guiding geospatial data could also represent either an interdune or an older, eroded dune field (Figure 25). We classified the site as a wind erosional feature with a low

confidence level because analysts could not clearly determine the landform type from satellite imagery alone.

Figure 25. Satellite image of a remotely mapped wind erosional feature. The *yellow circle* represents the actual location of this wind erosional feature.

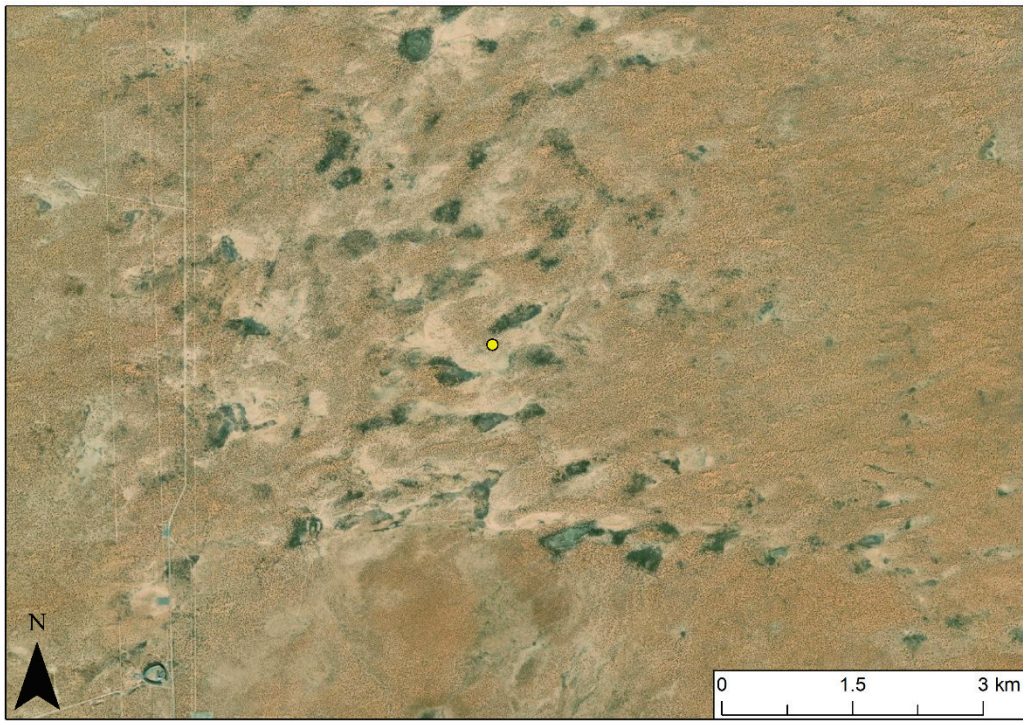

3.3.14 Agriculture

In dryland regions, producers often irrigate crops. In the satellite imagery, this creates a stark contrast between the green and light brown geometric shapes at the agricultural sites and the continuous darker brown and grayish colors typical of desert landscapes. As a result, our analysts were able to remotely map all 13 of our agricultural areas with high confidence. As shown in Figure 26, the style of agriculture in these locations varied between circular and rectangular fields, while other areas contained a mix of crop configuration styles.

Figure 26. Satellite image of a remotely mapped agricultural feature. The *yellow circle* represents the actual location of this agricultural feature.

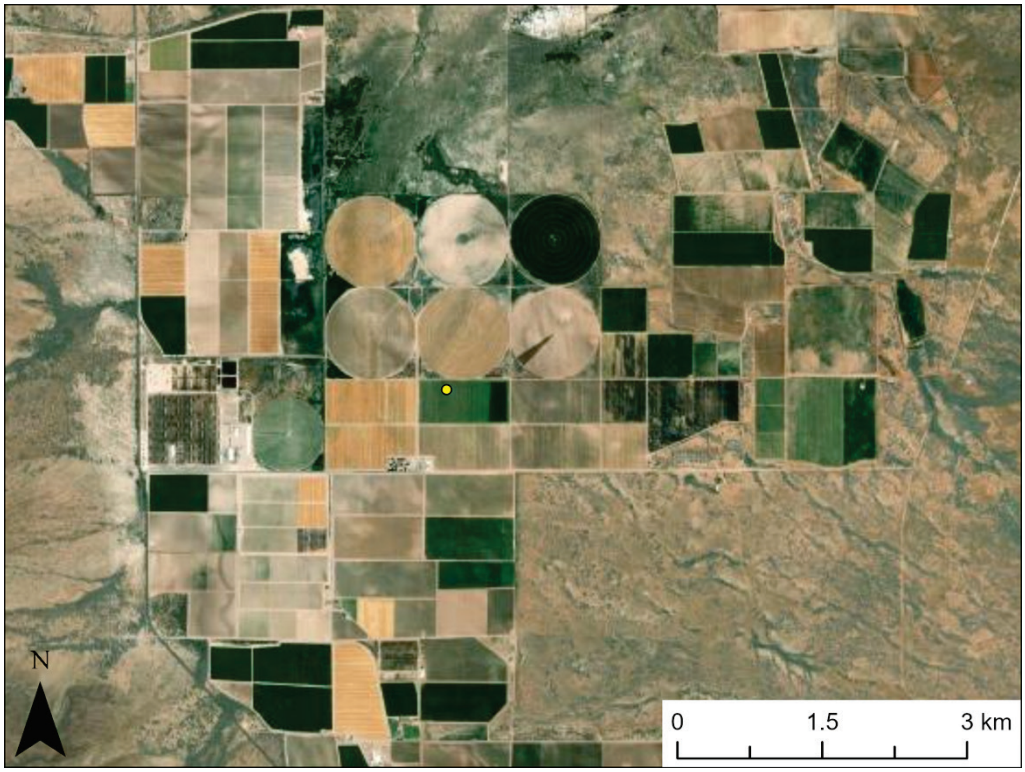

3.3.15 Bedrock

We labeled 11 bedrock locations remotely, with no additional field team assessments. Bedrock sites can have different expressions on the landscape, ranging from simply exposed and eroded bedding to crumbling structures (Figure 27). Our analysts labeled most of the bedrock locations with a high confidence level. However, two bedrock classifications located near landform boundaries had medium confidence levels, primarily due to their proximity to vegetated terrain.

Figure 27. Satellite image of a remotely mapped bedrock feature. The *yellow circle* represents the actual location of this bedrock feature.

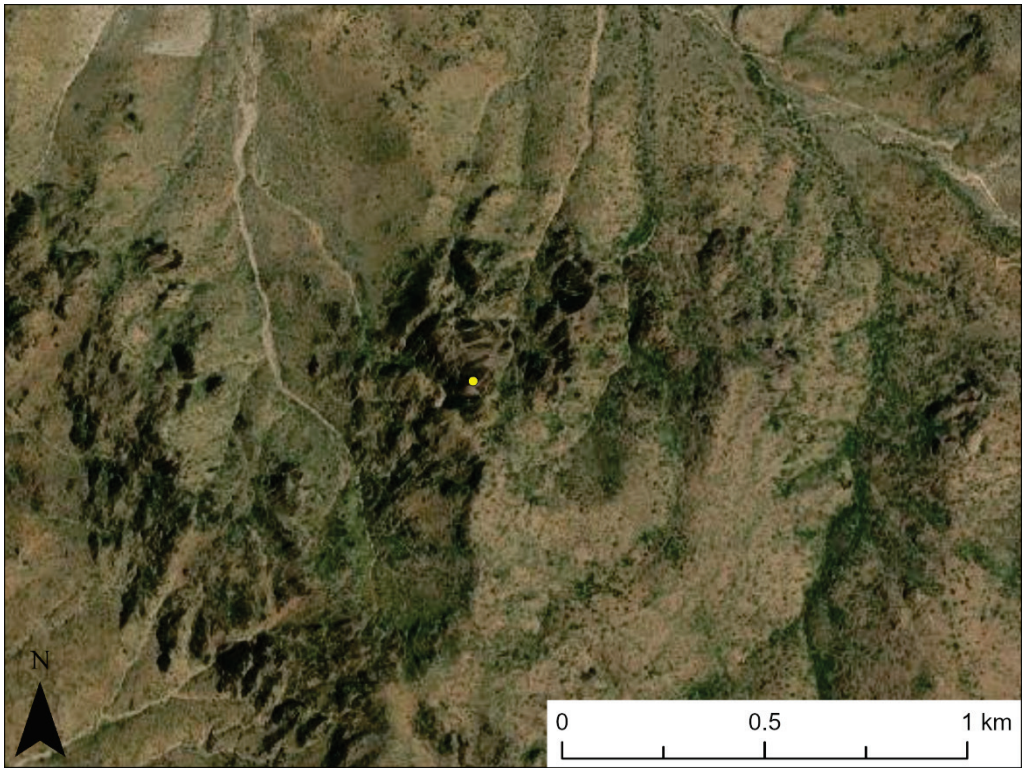

3.3.16 Fine-grained lake deposit

We remotely mapped eight fine-grained lake deposit field sites with no additional in situ assessments. When examining satellite imagery, it can be challenging to differentiate fine-grained lake deposits from playas. However, our analysts were able to confirm all eight locations considered for this study by reviewing secondary sources (e.g., Holliday et al. 2019). Figure 28 shows a portion of the largest fine-grained lake deposit landform that we recorded for this study. Given the secondary-source confirmations, our analysts classified all eight locations with a high level of confidence.

Figure 28. Satellite image of a remotely mapped fine-grained lake deposit that was confirmed by a secondary source. The *yellow circle* represents the actual location of the fine-grained lake deposit.

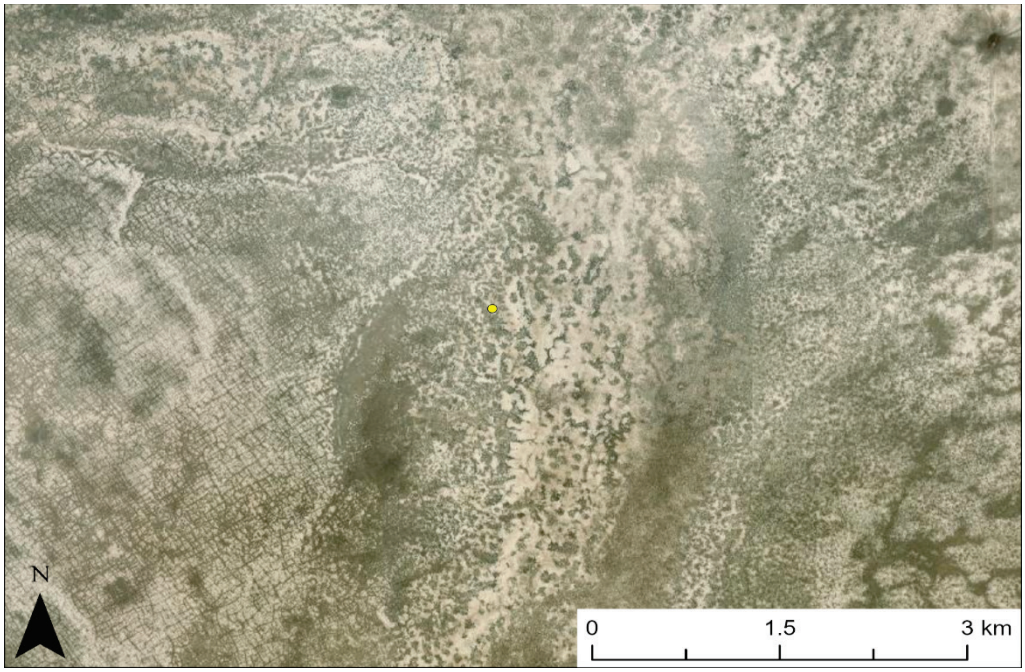

3.3.17 Urban

Urban areas are relatively easy to identify through remote mapping due to their high density of infrastructure (Figure 29). Our analysts recorded 10 urban areas via satellite imagery interpretation with a high level of confidence. No field assessments were necessary for the urban class.

Figure 29. Satellite image of a remotely mapped urban location. The *yellow circle* represents the relative center of the site.

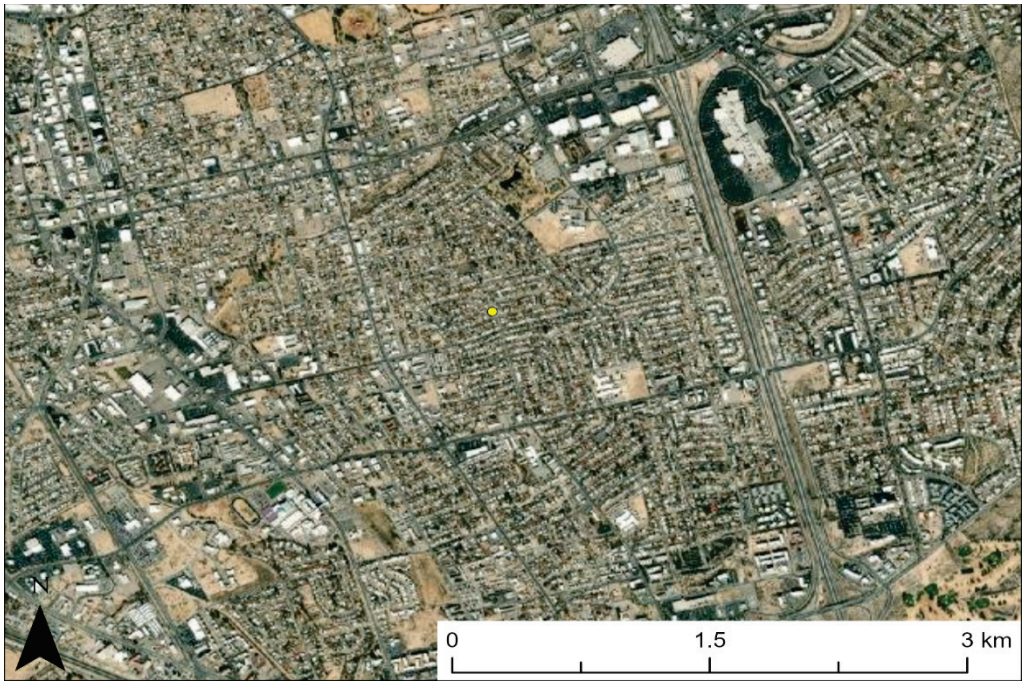

3.3.18 Water

Water locations are also relatively easy to identify through visual inspection of satellite imagery (Figure 30). For this effort, we remotely mapped nine sites with high confidence and confirmed that all nine sites were permanent, year-round water bodies rather than seasonally ephemeral features. Analysts determined this by examining the Esri basemap satellite imagery at multiple resolutions, with different map scales rendered from data collected over different dates and times to ensure minimal change in feature outlines through time (Figure 31).

Figure 30. Satellite image of a remotely mapped water feature. The *yellow circle* represents the actual location of this water feature.

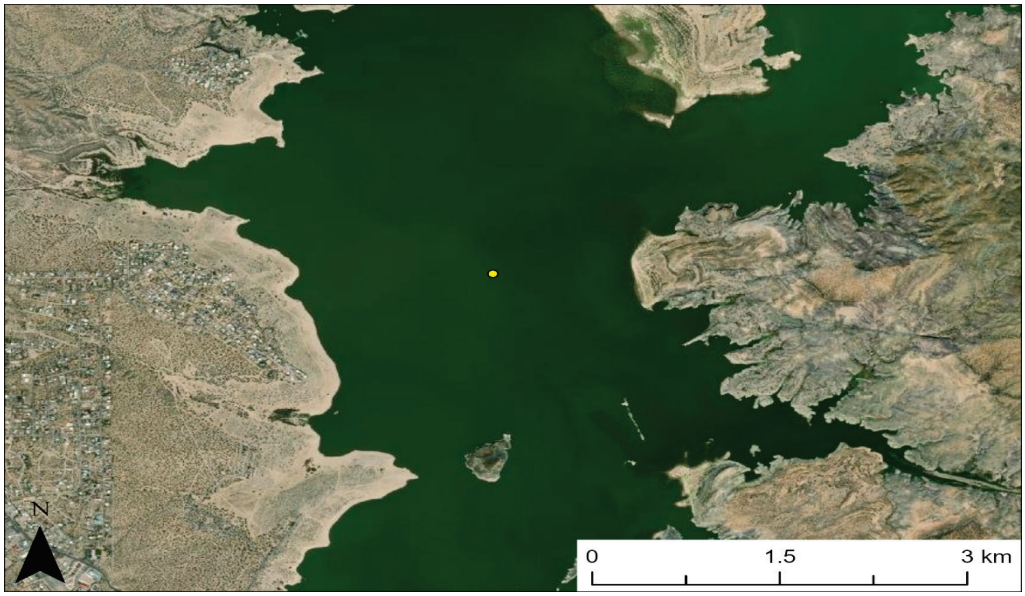

Figure 31. Water features at different map scales showing changes in feature dimensions, or lack thereof, through time. The two *upper* panels depict the same general region at two different resolutions. At a coarser map scale (*top left*), a water feature is depicted, while at a finer map scale (*top right*), a salt flat is depicted. Conversely, the two *bottom* panels depict a water feature that has roughly the same dimensions at both coarse and fine map resolutions, which suggests it is a permanent water feature.

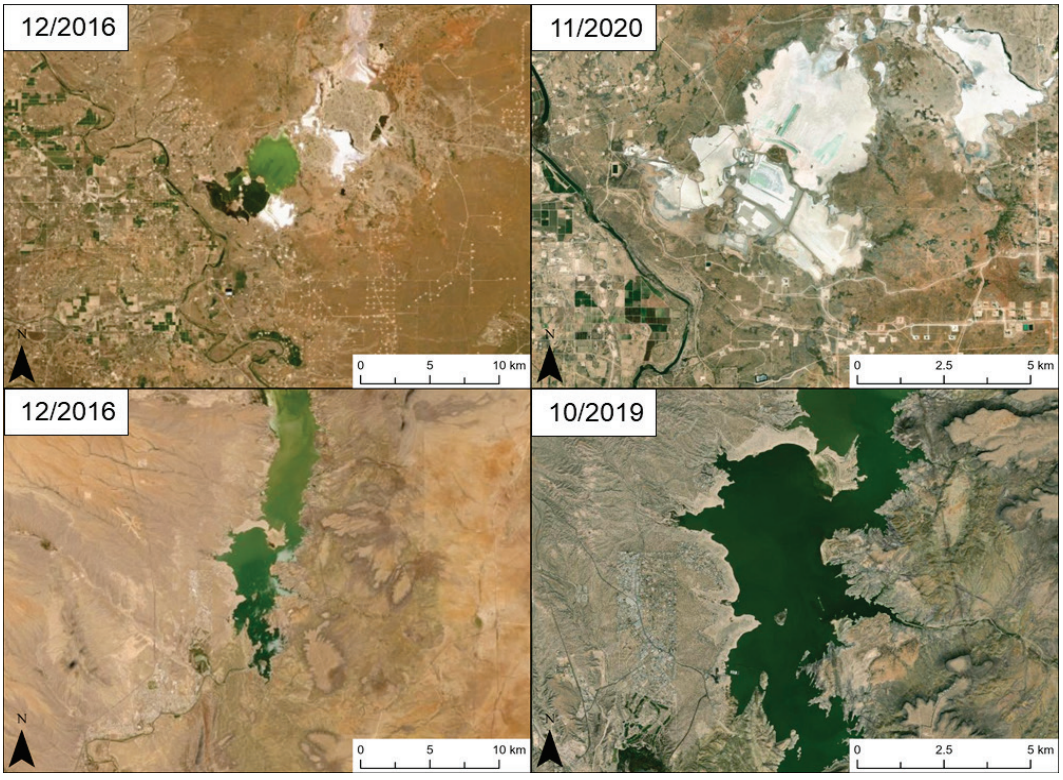

3.4 Independent reference landform data set

Table 6 shows the final reference landform data set, including all 128 landforms examined remotely and in person. Here, we provide labels according to both our reference scheme and the adapted McDonald, Adams, et al. (2020) scheme. This final data set will be critical for future work focused on evaluating and refining landform classification models to support dust-source characterization and land-management applications.

Table 6. Final independent reference landform data set mapped in this study. All landforms mapped remotely and in person are listed and compared to their respective McDonald, Adams, et al. (2020) SWUS landform map classification. The four landforms the field team deemed incorrectly classified are marked with an asterisk, and the alternative landform-type designation suggested by the field team is listed. The two alluvial plain sites with asterisks were originally misclassified as a fluvial terrace and a pediment, while the two bedrock sites with asterisks were originally misclassified as badlands and a fluvial terrace.

Latitude (DD)	Longitude (DD)	Study Classification	Classification Method	Confidence Level	McDonald, Adams, et al. (2020) SWUS Landform Map Classification
32.6063	−106.33	Sand dune	Remote	Medium	Sand dune
32.8216	−106.2729	Sand dune	In situ	High	Sand dune
32.7009	−106.232	Sand dune	In situ	Low	Sand dune
32.8182	−106.2575	Interdune	In situ	High	Sand dune
32.8194	−106.2775	Interdune	In situ	High	Sand dune
32.2429	−106.143	Sand sheet	Remote	High	Sand sheet
32.6849	−106.717	Sand sheet	Remote	High	Sand sheet
32.5682	−106.803	Sand sheet	Remote	High	Sand sheet
32.1813	−107.253	Sand sheet	Remote	High	Sand sheet
32.6037	−106.04	Sand sheet	In situ	High	Sand sheet
32.1437	−107.2449	Sand sheet	In situ	High	Sand sheet
32.1355	−107.236	Sand sheet	In situ	High	Sand sheet
32.2473	−106.6609	Sand plain	In situ	High	Sand sheet
32.4592	−108.597	Alluvial fan	Remote	High	Alluvial fan
32.5135	−106.83	Alluvial fan	Remote	Medium	Alluvial fan
30.9926	−105.0395	Alluvial fan	Remote	High	Alluvial fan
30.9312	−104.985	Alluvial fan	Remote	High	Alluvial fan
29.8824	−103.6466	Alluvial fan	Remote	High	Alluvial fan
29.8966	−103.6733	Alluvial fan	Remote	High	Alluvial fan
32.0462	−107.707	Alluvial fan	In situ	High	Alluvial fan
32.347	−106.6216	Alluvial fan	In situ	High	Alluvial fan
32.3998	−106.6103	Alluvial fan	In situ	High	Alluvial fan
32.8063	−105.9419	Alluvial fan	In situ	High	Alluvial fan

Table 6 (cont.). Final independent reference landform data set mapped in this study. All landforms mapped remotely and in person are listed and compared to their respective McDonald, Adams, et al. (2020) SWUS landform map classification. The four landforms the field team deemed incorrectly classified are marked with an asterisk, and the alternative landform-type designation suggested by the field team is listed. The two alluvial plain sites with asterisks were originally misclassified as a fluvial terrace and a pediment, while the two bedrock sites with asterisks were originally misclassified as badlands and a fluvial terrace.

Latitude (DD)	Longitude (DD)	Study Classification	Classification Method	Confidence Level	McDonald, Adams, et al. (2020) SWUS Landform Map Classification
30.8878	−105.144	Alluvial fan	Remote	High	Alluvial fan
32.1835	−106.586	Alluvial fan	Remote	High	Alluvial fan
30.9668	−104.901	Alluvial fan	Remote	High	Alluvial fan
32.5414	−106.826	Alluvial plain	Remote	High	Alluvial plain
32.1519	−107.538	Alluvial plain	Remote	High	Alluvial plain
32.4351	−108.674	Alluvial plain	In situ	High	Alluvial plain
33.3431	−105.943	Alluvial plain	In situ	High	Alluvial plain
32.0145	−106.5208	Alluvial plain	In situ	High	Alluvial plain
32.5414	−106.8259	Alluvial plain	Remote	High	Alluvial plain
32.1172	−107.4159	Alluvial plain	In situ	High	Alluvial plain
32.0922	−107.4959	Alluvial plain	In situ	High	Alluvial plain
32.2659	−106.6912	Alluvial plain*	In situ	Low	Alluvial plain
32.2077	−108.096	Alluvial plain*	In situ	High	Alluvial plain
33.4085	−106.095	Fluvial terrace	Remote	High	Fluvial terrace
32.5327	−108.615	Fluvial terrace	Remote	Medium	Fluvial terrace
32.5566	−108.578	Fluvial terrace	Remote	Medium	Fluvial terrace
33.5214	−106.043	Fluvial terrace	In situ	High	Fluvial terrace
33.5205	−106.047	Fluvial terrace	In situ	High	Fluvial terrace
32.8174	−106.086	Playa	Remote	High	Playa
32.7978	−106.2118	Playa	In situ	High	Playa
32.6565	−106.0149	Playa	In situ	High	Playa
32.3706	−106.9802	Playa	In situ	High	Playa
32.2766	−108.88	Playa	In situ	High	Playa
32.4564	−106.719	Playa	In situ	High	Playa
32.1764	−107.2717	Playa	In situ	High	Playa
31.3469	−103.403	Playa	Remote	High	Playa
31.8613	−105.086	Playa	Remote	High	Playa
31.6515	−104.948	Playa	Remote	High	Playa

Table 6 (cont.). Final independent reference landform data set mapped in this study. All landforms mapped remotely and in person are listed and compared to their respective McDonald, Adams, et al. (2020) SWUS landform map classification. The four landforms the field team deemed incorrectly classified are marked with an asterisk, and the alternative landform-type designation suggested by the field team is listed. The two alluvial plain sites with asterisks were originally misclassified as a fluvial terrace and a pediment, while the two bedrock sites with asterisks were originally misclassified as badlands and a fluvial terrace.

Latitude (DD)	Longitude (DD)	Study Classification	Classification Method	Confidence Level	McDonald, Adams, et al. (2020) SWUS Landform Map Classification
31.9704	−105.09	Playa	Remote	High	Playa
32.0256	−105.067	Playa	Remote	High	Playa
32.3643	−106.98	Playa	Remote	High	Playa
32.3134	−108.888	Playa	Remote	High	Playa
32.3706	−108.914	Playa	Remote	High	Playa
33.5385	−106.056	Plateau	In situ	High	Plateau
29.9607	−103.5924	Plateau	Remote	High	Plateau
29.9957	−103.6086	Plateau	Remote	High	Plateau
30.0217	−103.5358	Plateau	Remote	High	Plateau
30.0063	−103.861	Plateau	Remote	High	Plateau
30.0177	−103.832	Plateau	Remote	High	Plateau
30.0183	−103.819	Plateau	Remote	High	Plateau
30.0119	−103.801	Plateau	Remote	High	Plateau
29.9565	−103.64	Plateau	Remote	High	Plateau
29.9612	−103.667	Plateau	Remote	High	Plateau
30.5244	−103.694	Plateau	Remote	High	Plateau
30.5803	−103.581	Plateau	Remote	High	Plateau
30.5835	−103.558	Plateau	Remote	High	Plateau
30.5841	−103.602	Plateau	Remote	High	Plateau
33.6893	−105.922	Recent volcanic feature	In situ	High	Recent volcanic feature
32.0657	−106.9784	Recent volcanic feature	In situ	High	Recent volcanic feature
32.4579	−106.484	Pediment	Remote	High	Pediment
32.0417	−106.516	Pediment	Remote	Medium	Pediment
32.5579	−106.108	Wind erosional feature	Remote	Low	Wind erosional feature
32.5966	−104.415	Agriculture	Remote	High	Agriculture
32.5831	−104.444	Agriculture	Remote	High	Agriculture
32.6206	−104.38	Agriculture	Remote	High	Agriculture

Table 6 (cont.). Final independent reference landform data set mapped in this study. All landforms mapped remotely and in person are listed and compared to their respective McDonald, Adams, et al. (2020) SWUS landform map classification. The four landforms the field team deemed incorrectly classified are marked with an asterisk, and the alternative landform-type designation suggested by the field team is listed. The two alluvial plain sites with asterisks were originally misclassified as a fluvial terrace and a pediment, while the two bedrock sites with asterisks were originally misclassified as badlands and a fluvial terrace.

Latitude (DD)	Longitude (DD)	Study Classification	Classification Method	Confidence Level	McDonald, Adams, et al. (2020) SWUS Landform Map Classification
32.9484	−104.417	Agriculture	Remote	High	Agriculture
32.9592	−104.529	Agriculture	Remote	High	Agriculture
31.9269	−105.192	Agriculture	Remote	High	Agriculture
31.227	−103.645	Agriculture	Remote	High	Agriculture
33.889	−106.861	Agriculture	Remote	High	Agriculture
34.0259	−106.872	Agriculture	Remote	High	Agriculture
32.5245	−107.373	Agriculture	Remote	High	Agriculture
32.5724	−107.304	Agriculture	Remote	High	Agriculture
32.1826	−106.744	Agriculture	Remote	High	Agriculture
32.2428	−106.799	Agriculture	Remote	High	Agriculture
31.7317	−106.509	Urban	Remote	High	Urban
31.7738	−106.295	Urban	Remote	High	Urban
31.9097	−106.42	Urban	Remote	High	Urban
31.6152	−106.343	Urban	Remote	High	Urban
32.3018	−106.757	Urban	Remote	High	Urban
32.3115	−106.792	Urban	Remote	High	Urban
31.4206	−103.496	Urban	Remote	High	Urban
31.0441	−104.832	Urban	Remote	High	Urban
32.2587	−107.758	Urban	Remote	High	Urban
34.0651	−106.901	Urban	Remote	High	Urban
31.9332	−103.924	Water	Remote	High	Water
32.5497	−104.383	Water	Remote	High	Water
33.2083	−107.188	Water	Remote	High	Water
33.2821	−107.161	Water	Remote	High	Water
32.9309	−107.298	Water	Remote	High	Water
30.9634	−103.719	Water	Remote	High	Water
33.2985	−105.688	Water	Remote	High	Water
33.3216	−105.686	Water	Remote	High	Water
33.5991	−107.048	Water	Remote	High	Water
32.5345	−108.622	Bedrock*	Remote	Low	Bedrock

Table 6 (cont.). Final independent reference landform data set mapped in this study. All landforms mapped remotely and in person are listed and compared to their respective McDonald, Adams, et al. (2020) SWUS landform map classification. The four landforms the field team deemed incorrectly classified are marked with an asterisk, and the alternative landform-type designation suggested by the field team is listed. The two alluvial plain sites with asterisks were originally misclassified as a fluvial terrace and a pediment, while the two bedrock sites with asterisks were originally misclassified as badlands and a fluvial terrace.

Latitude (DD)	Longitude (DD)	Study Classification	Classification Method	Confidence Level	McDonald, Adams, et al. (2020) SWUS Landform Map Classification
33.1726	−105.897	Bedrock*	Remote	Low	Bedrock
32.79	−106.566	Bedrock	Remote	High	Bedrock
32.8904	−106.58	Bedrock	Remote	High	Bedrock
32.7685	−108.614	Bedrock	Remote	Medium	Bedrock
33.084	−108.482	Bedrock	Remote	Medium	Bedrock
31.9977	−104.898	Bedrock	Remote	High	Bedrock
32.0779	−104.904	Bedrock	Remote	High	Bedrock
32.1056	−104.966	Bedrock	Remote	High	Bedrock
33.7722	−106.217	Bedrock	Remote	High	Bedrock
32.1128	−107.63	Bedrock	Remote	High	Bedrock
32.1073	−107.628	Bedrock	Remote	High	Bedrock
32.0733	−107.638	Bedrock	Remote	High	Bedrock
33.8086	−108.268	Fine-grained lake deposit	Remote	High	Fine-grained lake deposit
33.8329	−108.194	Fine-grained lake deposit	Remote	High	Fine-grained lake deposit
33.8372	−108.093	Fine-grained lake deposit	Remote	High	Fine-grained lake deposit
33.9267	−107.791	Fine-grained lake deposit	Remote	High	Fine-grained lake deposit
32.5933	−103.753	Fine-grained lake deposit	Remote	High	Fine-grained lake deposit
32.5713	−103.696	Fine-grained lake deposit	Remote	High	Fine-grained lake deposit
32.5563	−103.773	Fine-grained lake deposit	Remote	High	Fine-grained lake deposit
32.6751	−103.961	Fine-grained lake deposit	Remote	High	Fine-grained lake deposit

4 Conclusions and Recommendations

Through in situ observations and remote satellite interpretation, we mapped a total of 128 landform sites, including 18 landform types, in the Chihuahuan Desert regions of Mexico and the United States. The ease with which analysts classified these landforms varied, which was evident in the confidence levels prescribed to each of the remotely mapped landforms and the reclassification of several landform types visited by the field crew.

The landforms that were easily identified by our mapping team were sand sheets, sand plains, alluvial fans, alluvial plains, playas, plateaus, recent volcanic features, urban, water, bedrock, and agriculture. In general, these particular landforms have pronounced, identifiable characteristics that are easy to see in satellite imagery. For example, alluvial fans are apparent by their classic leaf or lobate morphology, while playas are often expressed as minimally vegetated, flat, oval-shaped features on basin floors. Plateaus have characteristic high-relief and flat tops with steep drop-offs, and recent volcanic features are usually recognizable by their dark color that often contrasts with the surrounding landscape. Identifying exposed bedrock along mountaintops and ridges is also generally straightforward, provided it is minimally vegetated. Water sources are discernable but may require additional examination to determine if they are ephemeral or permanent in aeolian environments. Urban and agriculture are arguably the two most easily recognizable classes because both are products of marked alterations to the natural environment that make them clearly discernable from the surrounding landscape. Sand sheets and sand plains are often expressed as expansive, flat, sandy features but are easily distinguishable from low-gradient and extensive alluvial plains that are typically found in basin floors with visible flow patterns. The sand sheet and sand plain classes are challenging to discern from one another based solely on satellite imagery, but we effectively classified the sand plain and sand sheet classes as either one or the other with a high degree of certainty.

The most challenging landforms to label were sand dunes, interdunes, fluvial terraces, pediments, fine-grained lake deposits, badlands, and wind erosional features. Analysts noted that it was not uncommon to mistake fine-grained lake deposits for playas and suggested in-person confirmation to discern between the two when possible. While we were able to identify textbook examples of sand dunes and interdunes with relative ease, the older and stabilized dune features can be more difficult to decipher (Figure

32). In addition, both wind erosional features and sand dunes present some level of directionality and, as a result, can be hard to distinguish from one another without in-person observations.

Figure 32. *Top*: Stabilized sand dune, also shown in Fig. 6, that highlights the difficulty in deciphering between sand dunes, interdunes, and wind erosional features. *Bottom*: Pediment, also shown in Fig. 23, that displays the difficulty in differentiating pediments from fans, particularly without elevation data to support classification labels.

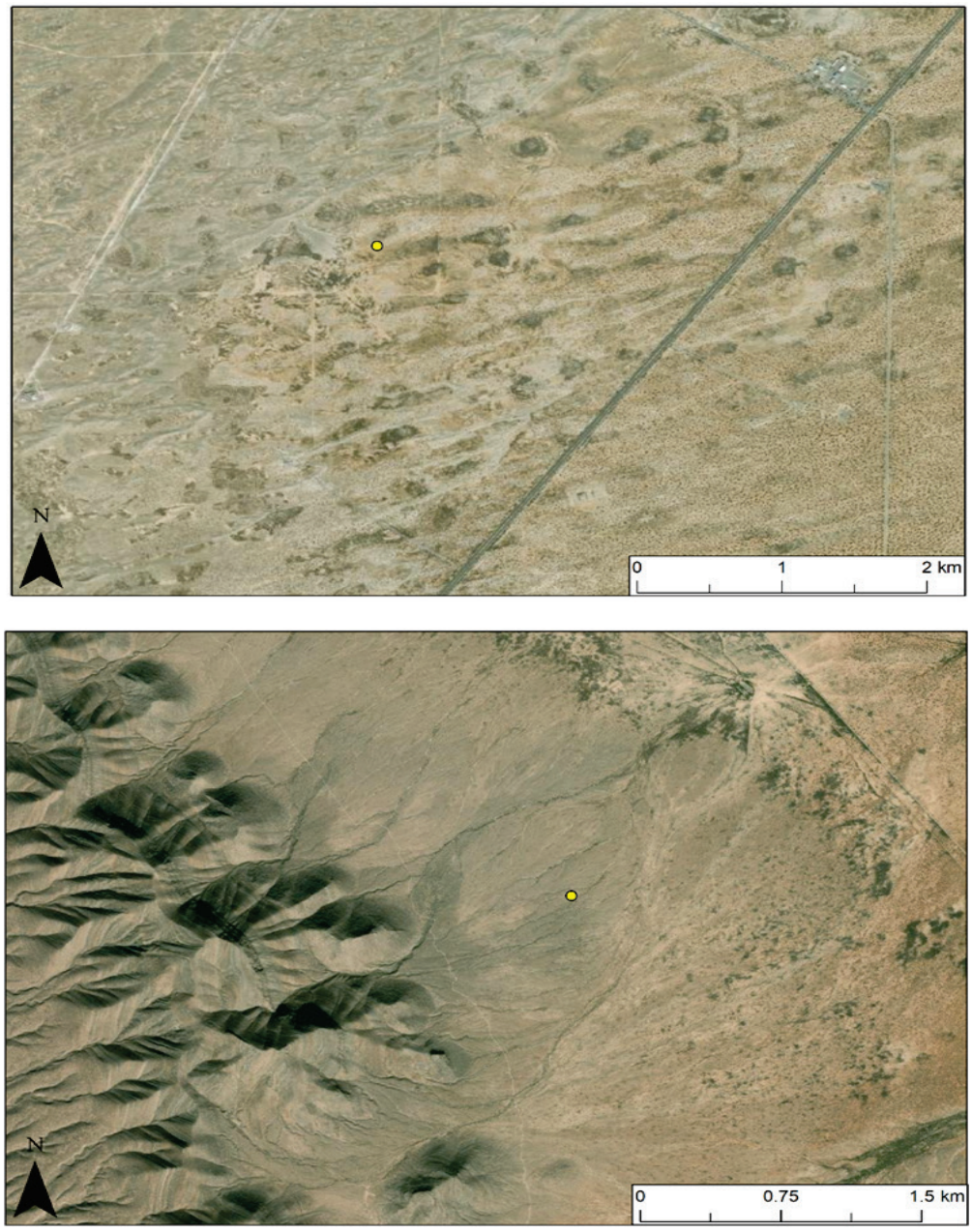

Some of the challenges of remote landform identification could be resolved by using high-fidelity (i.e., ≤10 m resolution) digital elevation model

(DEM) data. For example, fluvial terraces, though associated with pronounced stream networks, can be difficult to classify. Fluvial terraces are elevated above streams and flood plains, but it can be challenging to decipher exactly where that elevation step occurs using satellite imagery. Additional information about subtle changes in terrain slope would help analysts locate fluvial terrace landform boundaries. Badlands also exhibit topographic features that are difficult to see without high-fidelity data. We define badlands by their alternation between deep and narrow ephemeral washes and sharp and narrow ridge tops; these changes are more discernable with DEM data. DEM data could also help to distinguish alluvial fans, which tend to have steeper slopes, from more gently sloping pediments (Figure 32). Unfortunately, these subtle slope changes often cannot be discerned from publicly available DEM products (i.e., on the order of 30 m or coarser) and satellite imagery alone. Mappers require DEMs with resolutions of 10 m or finer to identify these subtle topographic variations, with finer (e.g., 1 m resolution) data preferred to capture smaller-scale elevation changes and drainage-channel patterns. For these reasons, we recommend that future reference data set expansion efforts consider supplementing in situ inspections and satellite-imagery-based assessments with high-resolution elevation data observations for landforms that are challenging to identify.

References

Bacon, S. N., and E. V. McDonald. 2016. "Regional Distribution of Salt-Rich Dust across Southwest Asia Based on Predictive Soil-Geomorphic Mapping Techniques." In *Military Geosciences and Desert Warfare*, edited by E. V. McDonald and T. Bullard, 237–256. New York: Springer. https://doi.org/10.1007/978-1-4939-3429-4_16.

Bacon, S. N., E. V. McDonald, R. Amit, Y. Enzel, and O. Crouvi. 2011. "Total Suspended Particulate Matter Emissions at High Friction Velocities from Desert Landforms." *Journal of Geophysical Research* 116 (F3), F03019. https://doi.org/10.1029/2011JF001965.

Bacon, S. N., E. V. McDonald, & H. L. Green. 2011. "Development of Geomorphic-Based Dust Source Emissions Data in Support of Forecasting Dust Storm Activity in Southwest Asia," In *Proceedings 9th International Conference on Military Geosciences, Abstracts with Programs*, 9–24 June 2011, Las Vegas, Nevada, 18.

Baddock, M. C., P. Ginoux, J. E. Bullard, and T. E. Gill. 2016. "Do MODIS-Defined Dust Sources Have a Geomorphological Signature?" *Geophysical Research Letters* 43 (6): 2606–2613. https://doi.org/10.1002/2015GL067327.

Bhattachan, A., G. S. Okin, J. Zhang, S. Vimal, and D. P. Lettenmaier. 2019. "Characterizing the Role of Wind and Dust in Traffic Accidents in California." *GeoHealth* 3 (10): 328–336. https://doi.org/10.1029/2019GH000212.

BLM (Bureau of Land Management). n.d. *Geospatial Business Platform: Assessment, Inventory, and Monitoring (AIM)*. US Department of the Interior. Accessed 01 July 2021. https://gbp-blm-egis.hub.arcgis.com/pages/aim.

Bullard, J., M. Baddock, G. McTainsh, and J. Leys. 2008. "Sub-Basin Scale Dust Source Geomorphology Detected Using MODIS." *Geophysical Research Letters* 35 (August): L15404. https://doi.org/10.1029/2008GL033928.

Bullard, J. E., S. P. Harrison, M. C. Baddock, N. Drake, T. E. Gill, G. McTainsh, and Y. Sun. 2011. "Preferential Dust Sources: A Geomorphological Classification Designed for Use in Global Dust-Cycle Models." *Journal of Geophysical Research* 116 (F4). https://doi.org/10.1029/2011JF002061.

De Longueville, F., Y.-C. Hountondji, S. Henry, and P. Ozer. 2010. "What Do We Know About Effects of Desert Dust on Air Quality and Human Health in West Africa Compared to Other Regions?" *Science of the Total Environment* 409 (1): 1–8. https://doi.org/10.1016/j.scitotenv.2010.09.025.

Department of the Army. 2019. *Intelligence Preparation of the Battlefield* ATP 2-01.3. Washington, DC: Department of the Army.

Esri, Maxar, Earthstar Geographics, CNES/Airbus DS, GeoEye, USDA FSA, USGS, Aerogrid, IGN, IGP, and the GIS User Community. (2021). *Imagery with Metadata*. Accessed 01 July 2021. https://www.arcgis.com/home/item.html?id=c03a526d94704bfb839445e80de95495.

Herrick, J. E., J. W. Van Zee, S. E. McCord, E. M. Courtright, J. W. Karl, and L. M. Burkett. 2017. *Monitoring Manual for Grassland, Shrubland, and Savanna Ecosystems. Vol. I: Core Methods*, 2nd ed. Las Cruces: USDA-ARS Jornada Experimental Range.

Hodgdon, T. S., R. E. Alter, S. L. LeGrand, and B. F. Morriss. 2021. *Enhanced Dust Emission Characterization for Improved Atmospheric Dust Forecasting; Task 1 Report: Training the Landform Inference Model*. Vicksburg, MS: US Army Corps of Engineers, Engineer Research and Development Center.

Holliday, V. T., A. Harvey, M. T. Cuba, and A. M. Weber. 2019. "Paleoindians, Paleolakes and Paleoplayas: Landscape Geoarchaeology of the Tularosa Basin, New Mexico." *Geomorphology* 331: 92–106. https://doi.org/10.1016/j.geomorph.2018.08.012.

LeGrand, S. L., and M. Brooks. 2018. *Sensitivity of Unified Model Dust Simulations to the ERDC-Geo Surface Erodibility Parameterization*. Vicksburg, MS: US Army Corps of Engineers, Engineer Research and Development Center.

McDonald, E., K. Adams, D. Page, E. Hartshorn, D. Sabol, and T. Wriston. 2020. *Summary of the Development of a Landform Map for the Western U.S. for Areas Prone to Dust Emission: Task 6A*. Reno, NV: Desert Research Institute.

McDonald, E., E. Hartshorn, M. Sweeney, and T. Lacey. 2020. *Quantifying PM10 and TSP Dust Emissions from Dust-Producing Landforms Common to the Desert Southwest U.S.: Task 6B*. Reno, NV: Desert Research.

Middleton, N. J. 2017. "Desert Dust Hazards: A Global Review." *Aeolian Research* 24: 53–63. https://doi.org/10.1016/j.aeolia.2016.12.001.

NPS (National Park Service). n.d. "Chihuahuan Desert Ecoregion." Accessed 10 August 2021. https://www.nps.gov/im/chdn/ecoregion.htm.

Okin, G. S., J. E. Bullard, R. L. Reynolds, J.-A. C. Ballantine, K. Schepanski, M. C. Todd, J. Belnap, M. C. Baddock, T. E. Gill, and M. E. Miller. 2011. "Dust: Small-Scale Processes with Global Consequences." *Eos, Transactions, American Geophysical Union* 92 (29): 241–242. https://doi.org/10.1029/2011EO290001.

Parajuli, S. P., Z.-L. Yang, and G. Kocurek. 2014. "Mapping Erodibility in Dust Source Regions Based on Geomorphology, Meteorology, and Remote Sensing." *Journal of Geophysical Research: Earth Surface* 119 (9): 1977–1994. https://doi.org/10.1002/2014JF003095.

Parajuli, S. P., and C. S. Zender. 2017. "Connecting Geomorphology to Dust Emission through High-Resolution Mapping of Global Land Cover and Sediment Supply." *Aeolian Research* 27 (August): 47–65. https://doi.org/10.1016/j.aeolia.2017.06.002.

Richter, D., and T. Gill. 2018. "Challenges and Opportunities in Atmospheric Dust Emission, Chemistry, and Transport." *Bulletin of the American Meteorological Society* 99 (7): ES115–ES118. https://doi.org/10.1175/BAMS-D-18-0007.1.

Rushingabigwi, G., P. Nsengiyumva, L. Sibomana, C. Twizere, and W. Kalisa. 2020. "Analysis of the Atmospheric Dust in Africa: The Breathable Dust's Fine Particulate Matter PM2.5 in Correlation with Carbon Monoxide." *Atmospheric Environment* 224: 117319. https://doi.org/10.1016/j.atmosenv.2020.117319.

Scarborough, R. 2000. "The Geologic Origin of the Sonoran Desert." In *A Natural History of the Sonoran Desert*, 1st ed., edited by S. J. Phillips and P. W. Comus. Oakland: University of California Press. http://www.desertmuseum.org/books/nhsd_geologic_origin.php.

Schoeneberger, P. J., and D. A. Wysocki. 2017. *Geomorphic Description System, Version 5.0*. Lincoln, NE: Natural Resources Conservation Service, National Soil Survey. https://www.nrcs.usda.gov/Internet/FSE_DOCUMENTS/nrcs142p2_051068.pdf

Schweitzer, M. D., A. S. Calzadilla, O. Salamo, A. Sharifi, N. Kumar, G. Holt, M. Campos, and M. Mirsaeidi. 2018. "Lung Health in Era of Climate Change and Dust Storms." *Environmental Research* 163: 36–42. https://doi.org/10.1016/j.envres.2018.02.001.

Sleeter, B. M., T. S. Wilson, and W. Acevedo, eds. 2012. *Status and Trends of Land Change in the Western United States–1973 to 2000*. Professional Paper 1794-A. Reston, VA: US Geological Survey. https://pubs.usgs.gov/pp/1794/a/pp1794a.pdf.

Sprigg, W. A., S. Nickovic, J. N. Galgiani, G. Pejanovic, S. Petkovic, M. Vujadinovic, A. Vukovic, et al. 2014. "Regional Dust Storm Modeling for Health Services: The Case of Valley Fever." *Aeolian Research* 14: 53–73. https://doi.org/10.1016/j.aeolia.2014.03.001.

Sweeney, M. R., E. V. McDonald, and V. Etyemezian. 2011. "Quantifying Dust Emissions from Desert Landforms, Eastern Mojave Desert, USA." *Geomorphology* 135 (1–2): 21–34. https://doi.org/10.1016/j.geomorph.2011.07.022.

USDA (US Department of Agriculture). n.d.a. "Description of SSURGO Database." Accessed 01 July 2021. https://www.nrcs.usda.gov/wps/portal/nrcs/detail/soils/survey/?cid=nrcs142p2_053627.

USDA (US Department of Agriculture). n.d.b. "National Soil Information System (NASIS)." Accessed 01 July 2021. https://www.nrcs.usda.gov/wps/portal/nrcs/detail/soils/survey/tools/?cid=nrcs142p2_053552

USDA (US Department of Agriculture). n.d.c. "Natural Resources Conservation Service." Accessed 10 August 2021. https://www.nrcs.usda.gov/wps/portal/nrcs/site/national/home/.

USGS (US Geological Survey). 2020. "Protected Areas Database of the United States (PAD-US) 2.1." US Geological Survey data release. https://doi.org/10.5066/P92QM3NT.

Wang, X., D. Xia, T. Wang, X. Xue, and J. Li. 2008. "Dust Sources in Arid and Semiarid China and Southern Mongolia: Impacts of Geomorphological Setting and Surface Materials." *Geomorphology* 97 (3–4): 583–600. https://doi.org/10.1016/j.geomorph.2007.09.006.

Wang, X., Z. Zhou, and Z. Dong. 2006. "Control of Dust Emissions by Geomorphic Conditions, Wind Environments and Land Use in Northern China: An Examination Based on Dust Storm Frequency from 1960 to 2003." *Geomorphology* 81 (3–4): 292–308. https://doi.org/10.1016/j.geomorph.2006.04.015.

Appendix: Landform Types in This Study

The figures that follow provide visual examples of all of the landform types mapped in this study. Each figure includes a satellite image and an associated description. To help delineate the landforms from surrounding landform assemblages, we outlined the approximate landform extent with red dashed lines in each image (excluding the sand dunes/interdunes and badlands figures due to the expansive nature of these landform types).

Figure A-1. Alluvial fans are "moderately- to gently-sloping constructional landforms that are composed of unconsolidated clastic sediment primarily derived from eroding highlands. The clastic materials typically consist of abundant gravel (>2 mm in diameter) and sand with lesser amounts of silt and clay. Alluvial fans typically occur on the upper margins of piedmont slopes that flank mountain highlands, plateaus, pediments, and badlands." (McDonald, Adams, et al. 2020, 13). The approximate extent of the landform is shown by the *red dashed line*.

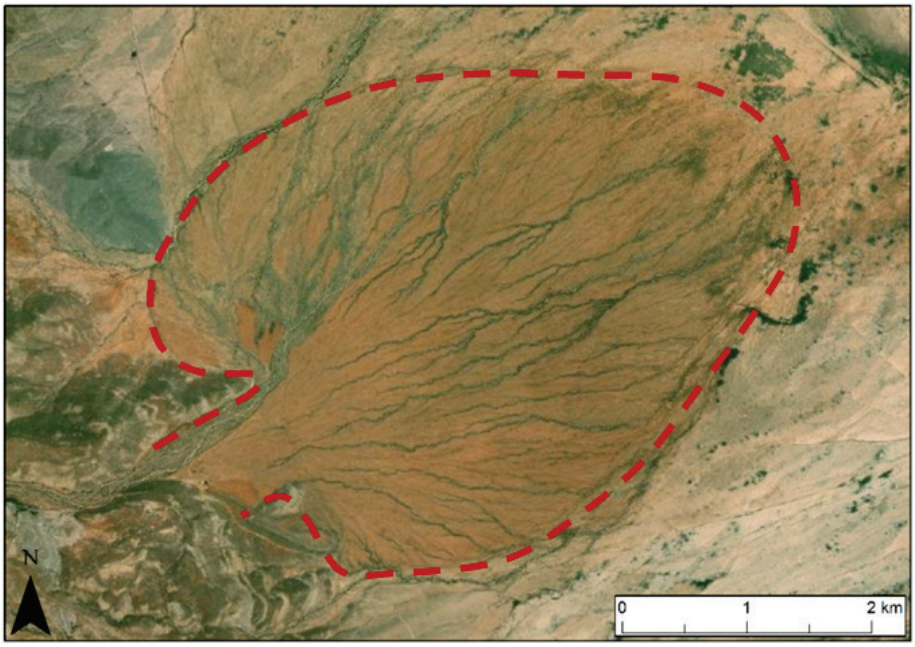

Figure A-2. Alluvial plains are "low-gradient landforms found along basin floors that are generally the floodplains of major axial streams. Deposits typically consist mostly of stratified, well- to moderately-sorted sand with lesser silt/clay and gravel. Sand sheets and sand sea/dunes often accumulate within alluvial plains downwind of playas. Vegetation cover is often found within the margins of alluvial plains along the banks of perennial or ephemeral streams or as isolated areas at alluvial fan and plain contacts associated with spring discharge" (McDonald, Adams, et al. 2020, 13). The approximate extent of the landform is shown by the area between the *red dashed lines*.

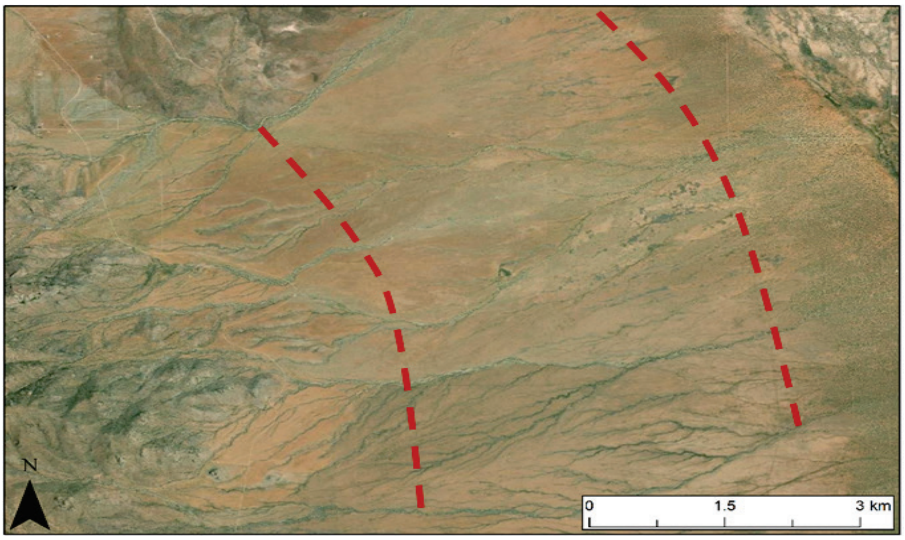

Figure A-3. A dune field showing sand dunes (white, wind-blown sand) and interdunes (tan sandy features separating the sand dunes). Sand dunes are "areas consisting of mounds, ridges, or hills of wind-blown sand, either bare or covered with vegetation, that are composed of loose and well-sorted sand and minor silt. Extensive areas of covered sand are referred to as sandy plains, dune fields or sand sea (also called ergs). These features occur where sand-rich sediment supply is plentiful" (McDonald, Adams, et al. 2020, 15). An interdune is "the relatively flat surface, whether sand-free or sand-covered, between dunes" (Schoeneberger and Wysocki 2017, 629-39).

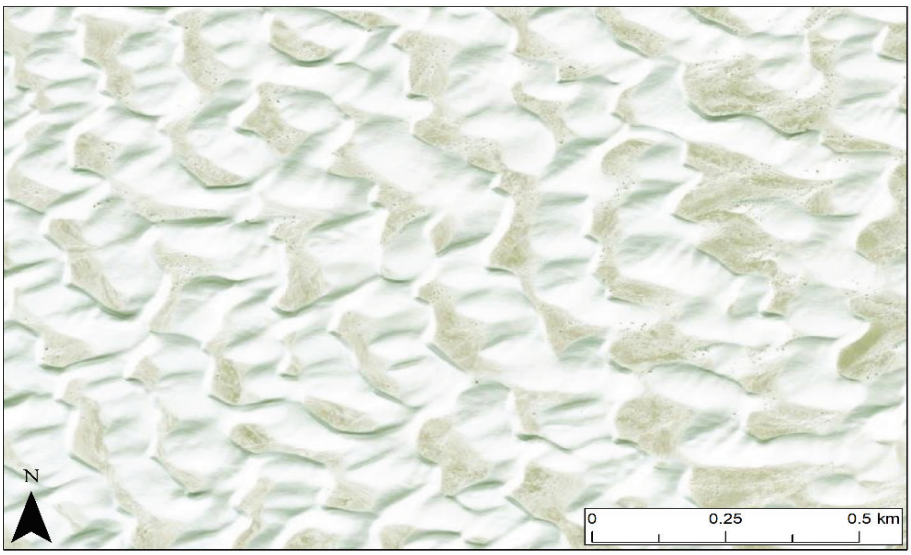

Figure A-4. Pediments are "erosional slopes or erosion surfaces that lie at the foot of mountain highlands or plateaus, which typically exhibit a concave upward profile. Pediment surfaces are typically broad and gently-sloping (2°–19°), cut into bedrock, commonly marginal to mountain highlands. Pediments may be bare or mantled with a thin layer of surficial sediment or rocks on the surface that form desert pavements" (McDonald, Adams, et al. 2020, 14). The approximate extent of the landform is shown by the area between the *red dashed lines*.

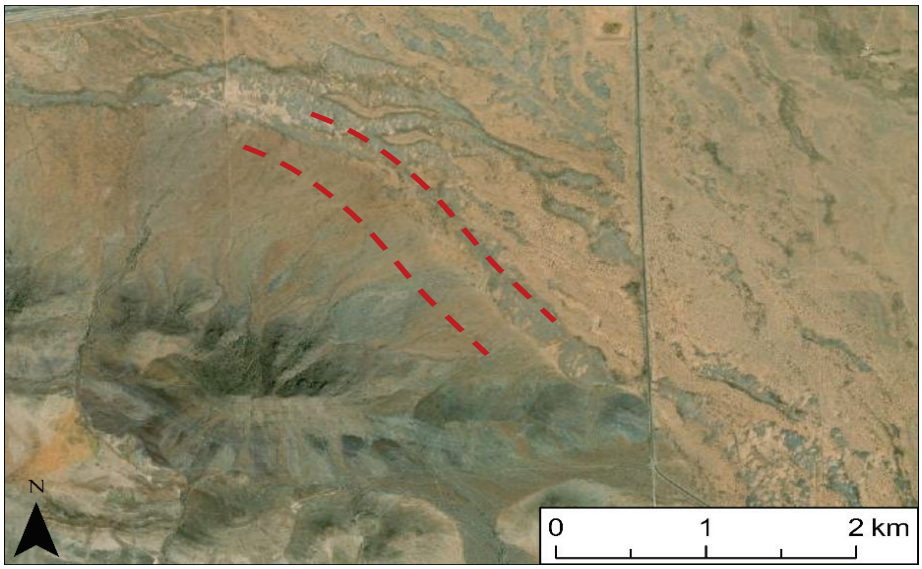

Figure A-5. A plateau is "a relatively elevated area of comparatively flat land composed of well-indurated bedrock, which is commonly limited on at least one side by an abrupt descent to lower ground. Plateaus form extensive areas of land that rise 150–300 m above the adjacent country or above sea level and commonly fringe mountain highlands. It is higher than a plain and more extensive than a mesa. Plateaus are commonly covered by a thin cap of silt-rich soil (loess)" (McDonald, Adams, et al. 2020, 14). The most distal edge of several plateaus is approximated by the *red dashed line*.

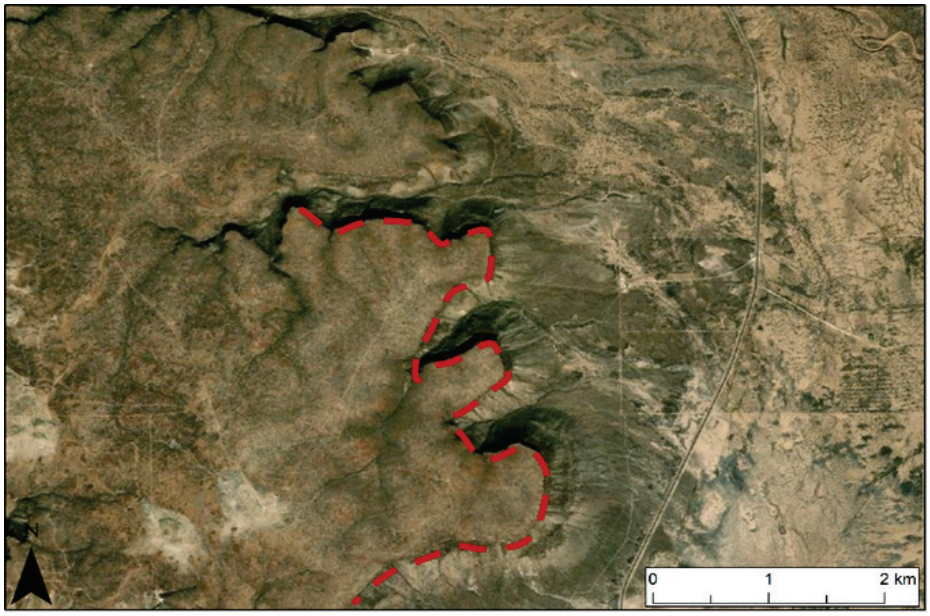

Figure A-6. A playa is "an ephemerally flooded, barren area on a basin floor that is characterized by fine-grained sedimentary deposition by floods in recent times and/or during previous pluvial episodes. Playas are typically located at the depocenter within a basin or lowland area" (McDonald, Adams, et al. 2020, 14). The approximate extent of the landform is shown by the *red dashed line*.

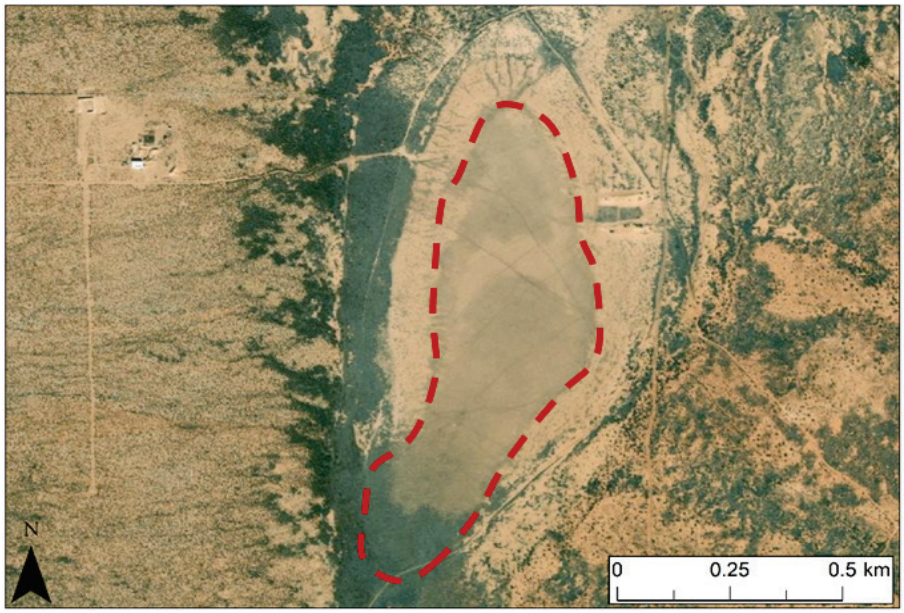

Figure A-7. Recent volcanic features are "landforms that have been recently formed from volcanic activity. The common type of recent volcanics is basalt flows and fields (plateaus) and volcanic vents (i.e., cinder cones, shield volcanos, lava flows, etc.)" (McDonald, Adams, et al. 2020, 15). The approximate extent of the landform is shown by the *red dashed line*.

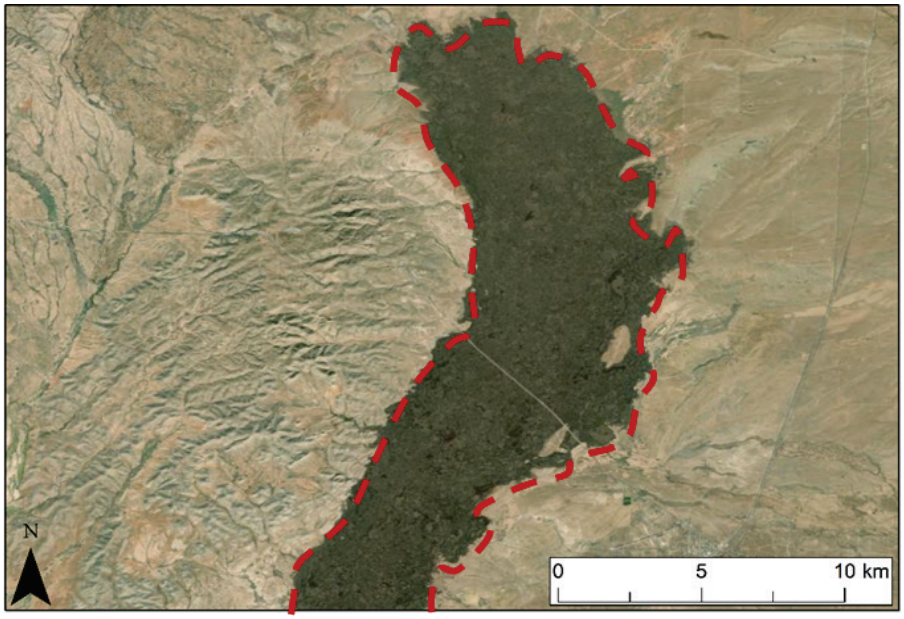

Figure A-8. A sand plain is "a sand-covered plain, which may originate by deflation of sand dunes, and whose lower limit of erosion is governed by the water table" (Schoeneberger and Wysocki 2017, 629-62). The approximate extent of the landform is shown by the *red dashed line*.

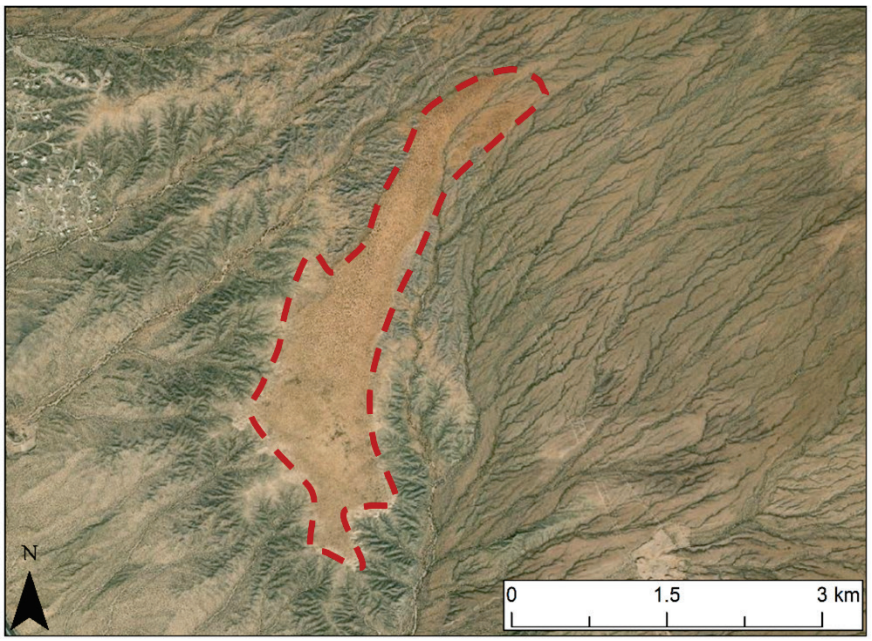

Figure A-9. Sand sheets are "sedimentary plains covered in fine sediments composed of loose and well-sorted sand to packed silt or clay. In systems of large linear dunes, these may include the troughs between dunes or may be associated with climbing dunes on alluvial fan surfaces" (McDonald, Adams, et al. 2020, 15). The approximate extent of the landform is contained within the *red dashed polygon*.

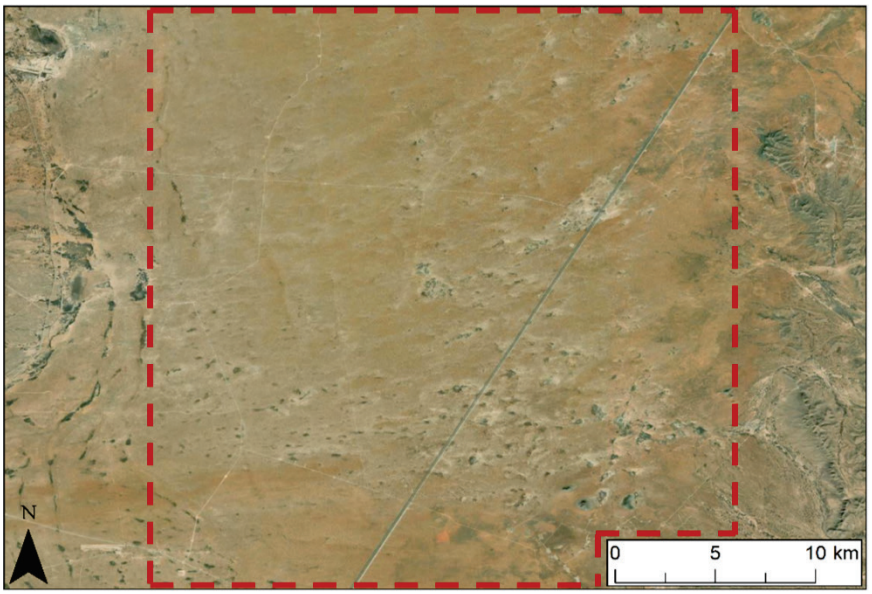

Figure A-10. Fluvial terraces are "stream or river terraces located adjacent to, but above, stream or river channels and flood plains" (McDonald, Adams, et al. 2020, 13). The approximate extent of the landform is shown by the area between the red dashed lines.

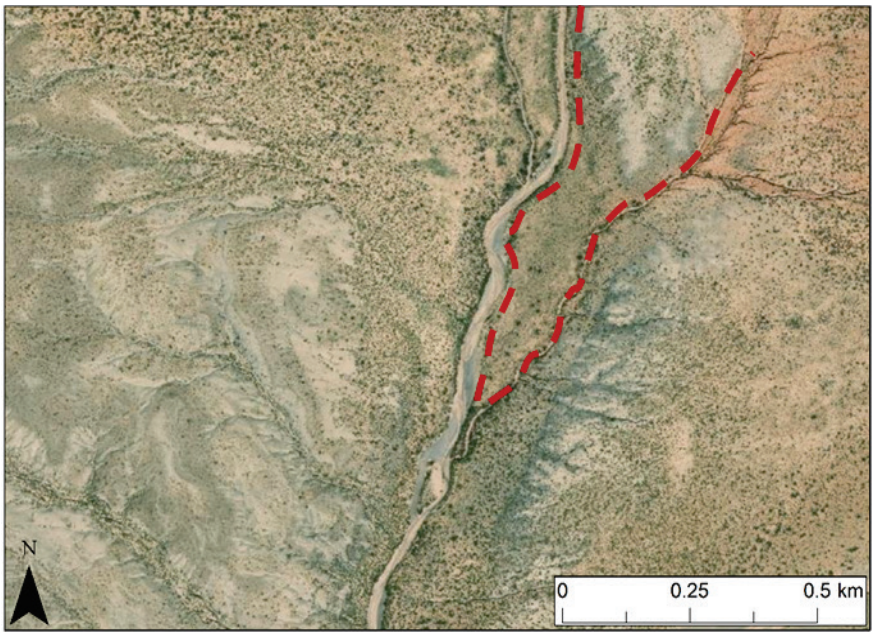

Figure A-11. Wind erosional features are "erosional features that typically exhibit an elongate ridge or series of ridges carved by wind erosion. The ridges are parallel to the prevailing wind direction and predominantly form on poorly- to moderately-consolidated sediment" (McDonald, Adams, et al. 2020, 15). The approximate extent of the landform is shown by the area within the rectangle delineated by the *red dashed line*.

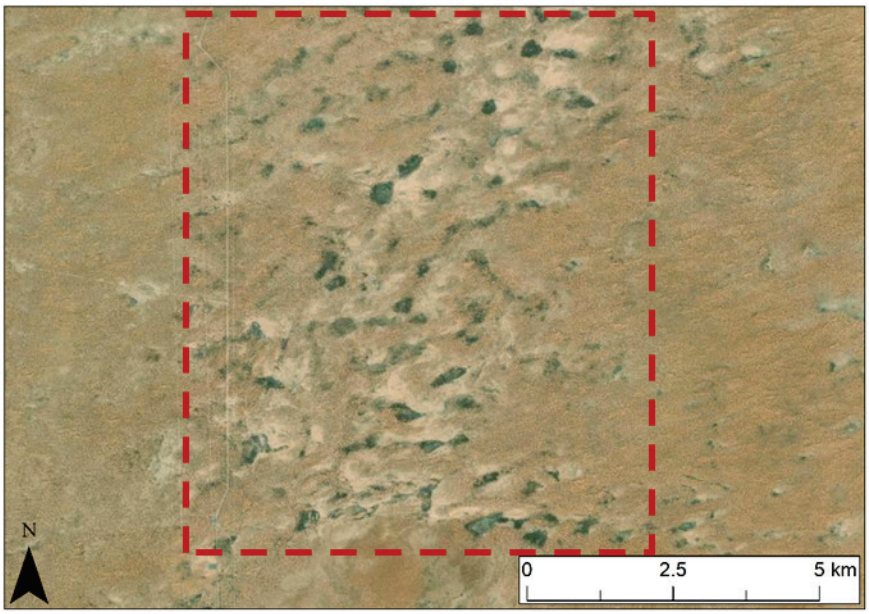

Figure A-12. Badlands: is “a landform that exhibits a complex stream-dissected topography consisting of deep, narrow ephemeral washes alternating with abundant, sharp and narrow ridge tops. Surfaces commonly have little or no vegetative cover, are highly erosive, and with no or minimal development of soils. Underlying material is generally unconsolidated or weakly indurated sediment largely composed of mixtures of clay, silt, and sand. Soluble salts of gypsum and halite are common” (McDonald, Adams, et al. 2020, 14). Badlands are highly expansive, and most of the image, excluding the river channels, displays badlands.

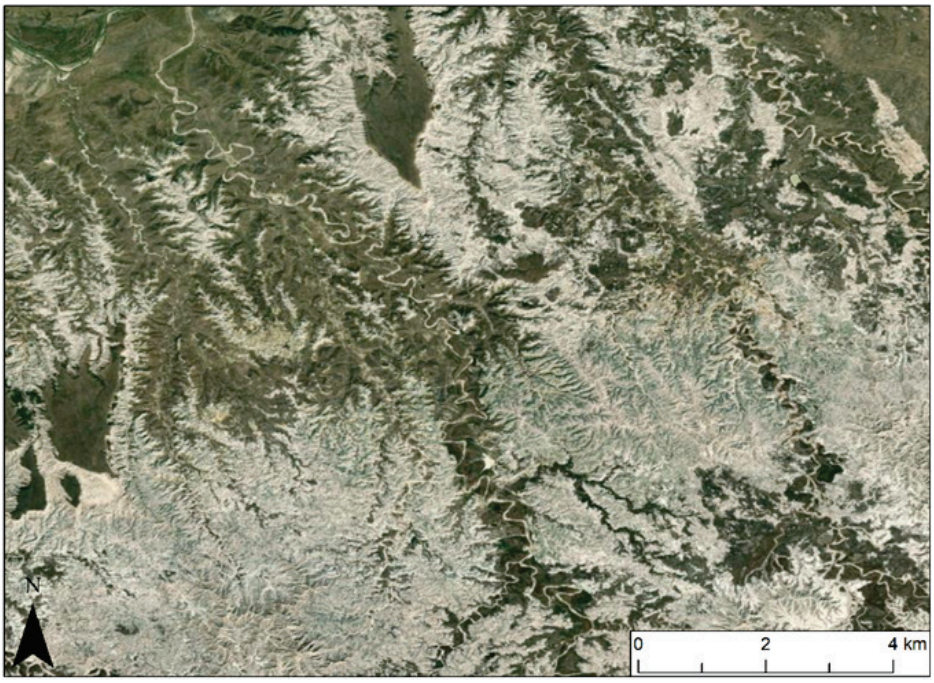

Figure A-13. Agriculture is defined as "a human-modified 'landscape' dominated by permanent, extensive alterations to the physical shape and/or internal stratigraphy of the land due to agricultural management for food, fiber or forage production, that have substantively altered water flow and sediment transport across and within the regolith (e.g., leveled land). Commonly excludes areas of minor alterations (e.g., shallow plowing) that are easily obscured or obliterated by natural bio-, pedo-, or cryoturbation" (Schoeneberger and Wysocki 2017, 629-4). The approximate extent of the agriculture area is shown by the *red dashed polygon*.

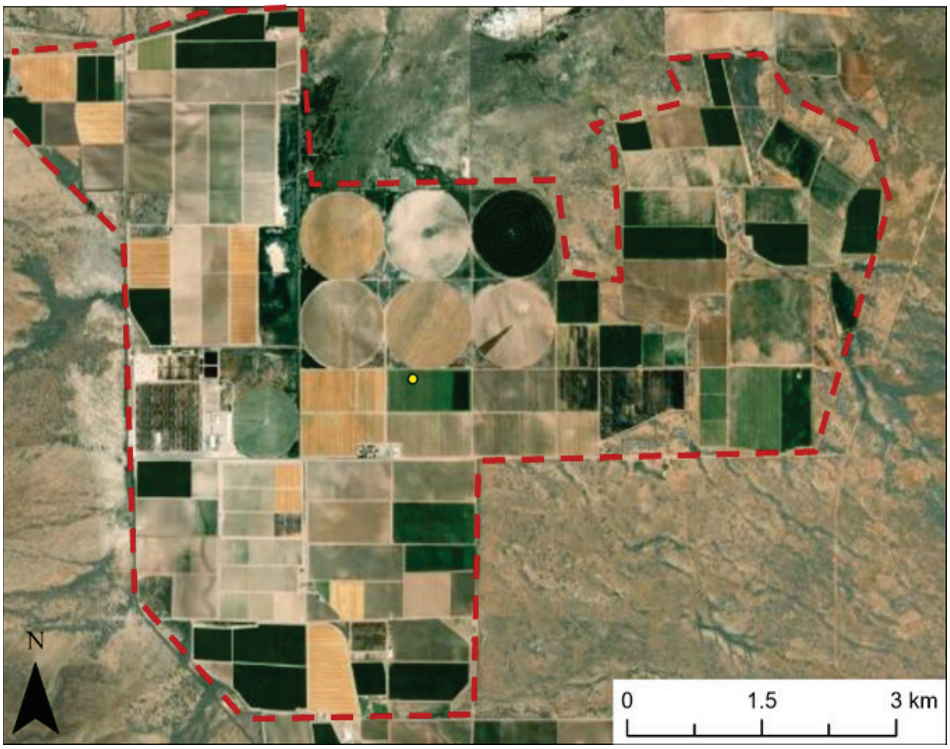

Figure A-14. Bedrock is "a general term for the solid rock that underlies the soil and other unconsolidated material or that is exposed at the surface" (Schoeneberger and Wysocki 2017, 629-10). The approximate extent of the bedrock area is shown by the *red dashed polygon*.

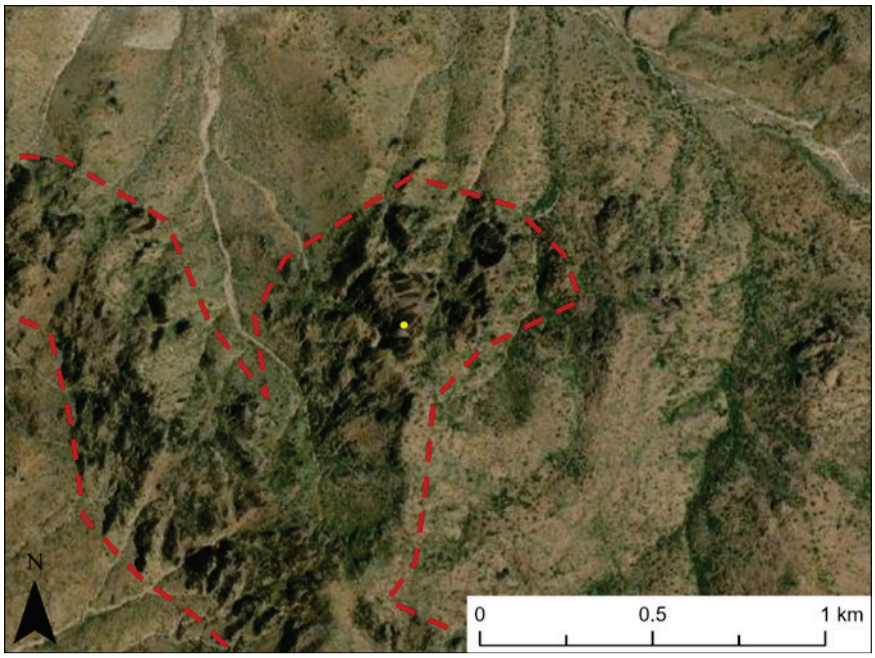

Figure A-15. Fine-grained lake deposits "are typically light colored, fine-grained (e.g., high silt and clay content) lake deposits found in basin bottoms and rimming playas. May or may not be eroded into badland forms" (McDonald, Adams, et al. 2020, 14). The approximate extent of the fine-grained lake deposit is shown by the *red dashed polygon*.

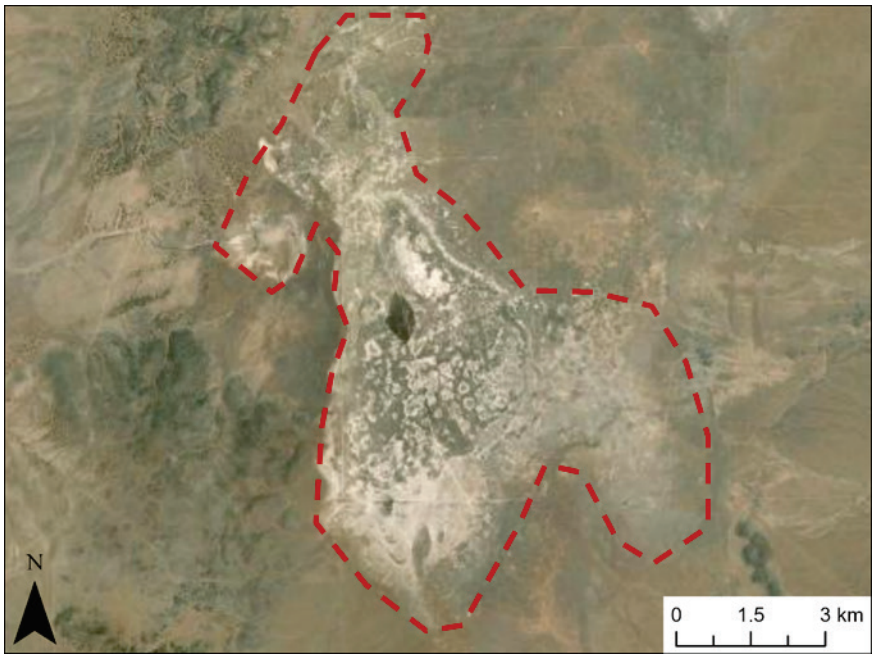

Figure A-16. Urban areas are "areas of extensive urban/suburban/industrial development where soil surface is modified and covered by buildings and infrastructure" (McDonald, Adams, et al. 2020, 16). The approximate extent of the urban area is shown by the *red dashed polygon*.

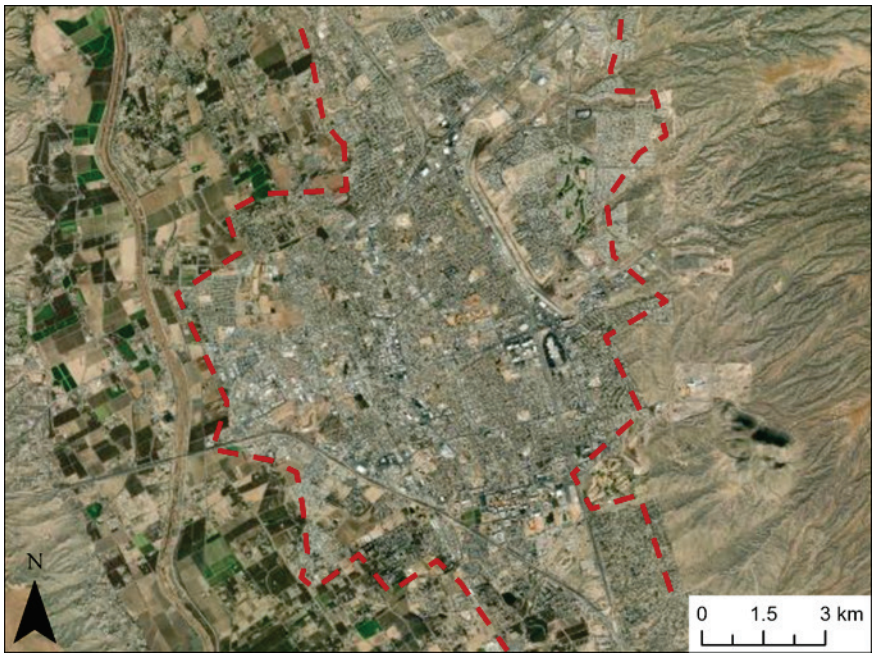

Figure A-17. Water refers to "open bodies of water including reservoirs, lakes, seas, and rivers" (McDonald, Adams, et al. 2020, 16). The approximate extent of the water feature is shown by the *red dashed polygon*.

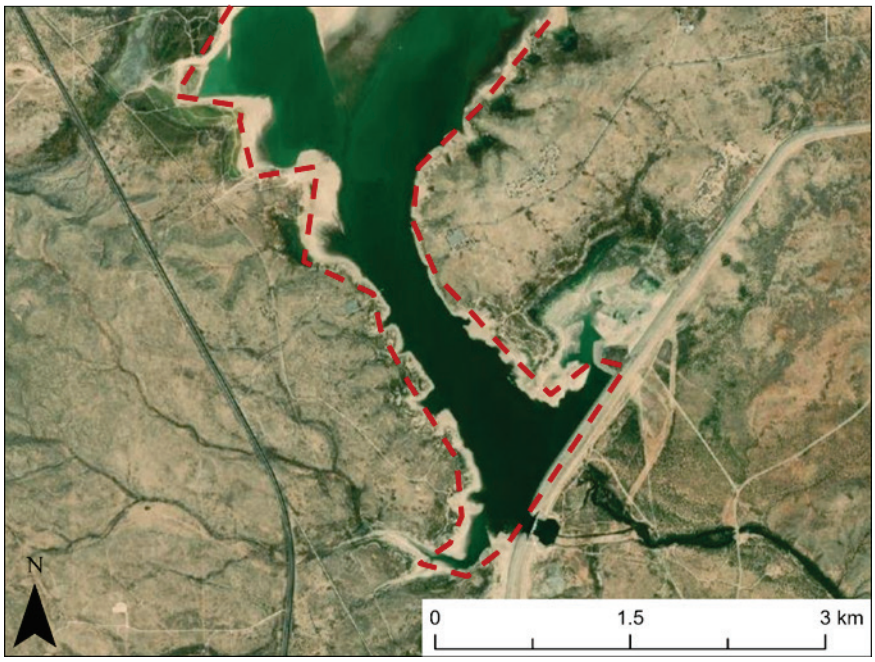

Abbreviations

AIM	Assessment, Inventory, and Monitoring
BLM	Bureau of Land Management
ERDC	Engineer Research and Development Center
DD	Decimal Degrees
DEM	Digital Elevation Model
GIS	Geographic Information System
ML	Machine Learning
NASIS	National Soil Information System
NRCS	Natural Resources and Conservation Service
PAD-US	Protected Areas Database of the United States
SME	Subject Matter Expert
SSURGO	Soil Survey Geographic Database
SWUS	Southwest United States

REPORT DOCUMENTATION PAGE

Form Approved
OMB No. 0704-0188

1. REPORT DATE (DD-MM-YYYY)	2. REPORT TYPE	3. DATES COVERED (From - To)
September 2022	Final	FY20–FY22

4. TITLE AND SUBTITLE

Landform Identification in the Chihuahuan Desert for Dust Source Characterization Applications: Developing a Landform Reference Data Set

5a. CONTRACT NUMBER

5b. GRANT NUMBER

5c. PROGRAM ELEMENT

6. AUTHOR(S)

Samantha N. Cook, Matthew F. Bigl, Sandra L. LeGrand, Nicholas Webb, Gayle Tyree, and Ronald Treminio

5d. PROJECT NUMBER

5e. TASK NUMBER

5f. WORK UNIT NUMBER

7. PERFORMING ORGANIZATION NAME(S) AND ADDRESS(ES)

US Army Engineer Research and Development Center (ERDC)
Cold Regions Research and Engineering Laboratory (CRREL)
72 Lyme Road
Hanover, NH 03755-1290

US Army Engineer Research and Development Center (ERDC)
Geospatial Research Laboratory (GRL)
7701 Telegraph Road
Alexandria, VA 22315-3864

8. PERFORMING ORGANIZATION REPORT NUMBER

ERDC TR-22-20

9. SPONSORING / MONITORING AGENCY NAME(S) AND ADDRESS(ES)

Air Force Life Cycle Management Center
75 Vandenberg Drive, Bldg 1630
Hanscom AFB, MA 01731-2103

10. SPONSOR/MONITOR'S ACRONYM(S)

11. SPONSOR/MONITOR'S REPORT NUMBER(S)

12. DISTRIBUTION / AVAILABILITY STATEMENT

Approved for public release; distribution is unlimited.

13. SUPPLEMENTARY NOTES

MIPR F2BDAN1239G003

14. ABSTRACT

ERDC-Geo is a surface erodibility parameterization developed to improve dust predictions in weather forecasting models. Geomorphic landform maps used in ERDC-Geo link surface dust emission potential to landform type. Using a previously generated southwest United States landform map as training data, a classification model based on machine learning (ML) was established to generate ERDC-Geo input data. To evaluate the ability of the ML model to accurately classify landforms, an independent reference landform data set was created for areas in the Chihuahuan Desert. The reference landform data set was generated using two separate mapping methodologies: one based on in situ observations, and another based on the interpretation of satellite imagery. Existing geospatial data layers and recommendations from local rangeland experts guided site selections for both in situ and remote landform identification. A total of 18 landform types were mapped across 128 sites in New Mexico, Texas, and Mexico using the in situ (31 sites) and remote (97 sites) techniques. The final data set is critical for evaluating the ML-classification model and, ultimately, for improving dust forecasting models.

15. SUBJECT TERMS

Chihuahuan Desert, Desert, Dust emission, Geomorphology, Geospatial data, Landforms, Machine learning, Remote sensing, Terrain characterization

16. SECURITY CLASSIFICATION OF:			17. LIMITATION OF ABSTRACT	18. NUMBER OF PAGES	19a. NAME OF RESPONSIBLE PERSON
a. REPORT	b. ABSTRACT	c. THIS PAGE			19b. TELEPHONE NUMBER (include area code)
Unclassified	Unclassified	Unclassified	SAR	80	